Chapter 4
Boundary Integral Equations and Their Approximations

The local problems in the definition of basis functions for the BEM-based FEM are treated by means of boundary integral equations. This chapter gives a short introduction into this topic with a special emphasis on its application in the BEM-based FEM. Therefore, the boundary integral operators for the Laplace problem are reviewed in two- and three-dimensions and corresponding boundary integral equations are derived. Their discretization is realized by a Galerkin boundary element method, which is used in the numerical examples and tests throughout the book. However, we also give an alternative approach for the discretization of boundary integral equations that relies on the Nyström method. The application of these approaches as local solvers for the BEM-based FEM is discussed in details and some comparisons highlighting advantageous and disadvantageous of these two solvers are given.

4.1 Preliminaries

Boundary element methods (BEM) are alternative approaches to finite element methods for the approximation of boundary value problems. They play an important role in modern numerical computations in the applied and engineering sciences. These methods rely on equivalent boundary integral equations of the corresponding boundary value problems, which are known in many cases. The key ingredient is the knowledge of a fundamental solution of the differential operator. Although the existence of such functions can be guarantied for a wide class of partial differential equations, see [100], the explicit construction is a more difficult task. However, the fundamental solution is known for important operators with constant coefficients such as for the Laplace and Helmholtz operators as well as for the system of elasticity and for Stokes equations, for instance. These include the most important applications of the boundary element methods. The advantage of the BEM over the

S. Weißer, *BEM-based Finite Element Approaches on Polytopal Meshes*,
Lecture Notes in Computational Science and Engineering 130,
https://doi.org/10.1007/978-3-030-20961-2_4

FEM is that the d-dimensional problems are reduced to $d-1$-dimensional ones on the boundary of the underlying domain. Furthermore, due to the formulation on the boundary, the BEM is naturally applicable for unbounded exterior domains, which are of particular interest in scattering problems, for example. When discretizing a boundary integral equation, we generally speak about a boundary element method. But, if it is referred to BEM in this book, we usually mean a Galerkin approach for the approximation of the boundary integral equation as described in Sect. 4.3. The Galerkin methods perfectly fit to the variational formulation of these integral equations. Their theoretical study is complete and provides a powerful tool for the analysis. In the engineering community, collocation methods are often preferred because of their easier practical implementation. However, the stability and convergence theory for these methods is only available for two-dimensional problems. Alternatively, a Nyström discretization of the boundary integral equation can be chosen, where the integrals of the operators are replaced by appropriate quadrature formulas. This strategy is discussed in Sect. 4.4. For more details on the theory of integral and in particular boundary integral equations we refer to the literature [13, 61, 105, 107, 118, 127, 128]. Galerkin boundary element methods are studied and discussed in [151, 158, 159] for elliptic differential operators. The collocation and Nyström approaches can be found beside others in [13, 118] and we especially mention [117, 133] for the Nyström discretizations.

In the following presentation, we restrict ourselves to the pure Laplace problem

$$-\Delta u = 0 \quad \text{in } K\,, \qquad u = g \quad \text{on } \partial K \tag{4.1}$$

with Dirichlet boundary conditions on a bounded polytopal domain K in two- and three-dimensions. Note that K will be a polytopal element and g a piecewise polynomial function in our application later on. This problem setting is sufficient for the approximation in the BEM-based FEM as seen in Sect. 4.5. The approach is also applicable to the before mentioned differential operators and in particular to convection-diffusion-reaction problems. Furthermore, other types of boundary conditions can be incorporated when needed, for instance, in Neumann or mixed boundary value problems. Some of the possible modifications are discussed in Chap. 6.

4.2 Boundary Integral Formulations

Let $K \subset \mathbb{R}^d$, $d = 2, 3$ be a bounded open domain with polygonal or polyhedral boundary, and we consider the boundary value problem (4.1) with some given function $g \in H^{1/2}(\partial K)$. For the following theory of boundary integral formulations, we need the usual trace operator γ_0^K. For sufficiently smooth functions, it is given as restriction of the function to the boundary. For Lipschitz domains, and thus in particular for polytopal domains, the trace is a bounded linear operator with $\gamma_0^K : H^s(K) \to H^{s-1/2}(\partial K)$ for $1/2 < s \leq 1$ and it has a continuous right inverse.

Here, the superscript indicates that the trace is taken with respect to the domain K. Let $v \in H^1(K)$ with Δv in the dual of $H^1(K)$. Due to Green's first identity [128], there exists a unique function $\gamma_1^K v \in H^{-1/2}(\partial K)$ such that

$$\int_K \nabla v(\mathbf{y}) \cdot \nabla w(\mathbf{y}) \, \mathrm{d}\mathbf{y} = \int_{\partial K} \gamma_1^K v(\mathbf{y}) \gamma_0^K w(\mathbf{y}) \, \mathrm{d}s_{\mathbf{y}} - \int_K w(\mathbf{y}) \Delta v(\mathbf{y}) \, \mathrm{d}\mathbf{y} \tag{4.2}$$

for $w \in H^1(K)$. We call $\gamma_1^K v$ the conormal derivative of v. If v is sufficiently smooth, e.g. $v \in H^2(K)$, we have

$$(\gamma_1^K v)(\mathbf{x}) = \mathbf{n}_K(\mathbf{x}) \cdot (\gamma_0^K \nabla v)(\mathbf{x}) \quad \text{for } \mathbf{x} \in \partial K \ ,$$

where $\mathbf{n}_K(\mathbf{x})$ denotes the outer normal vector of the domain K at $\mathbf{x}$. The trace and the conormal derivative are also called Dirichlet and Neumann trace for the Laplace equation. Additionally, we make use of the fundamental solution of the Laplacian. This singular function is given as

$$U^*(\mathbf{x}, \mathbf{y}) = \begin{cases} -\dfrac{1}{2\pi} \ln |\mathbf{x} - \mathbf{y}| & \text{for } \mathbf{x}, \mathbf{y} \in \mathbb{R}^2 \ , \\ \dfrac{1}{4\pi \, |\mathbf{x} - \mathbf{y}|} & \text{for } \mathbf{x}, \mathbf{y} \in \mathbb{R}^3 \ . \end{cases}$$

The fundamental solution satisfies the equation

$$-\Delta_{\mathbf{y}} U^*(\mathbf{x}, \mathbf{y}) = \delta_0(\mathbf{y} - \mathbf{x})$$

in the distributional sense, where δ_0 is the Dirac delta distribution. If we substitute $v(\mathbf{y}) = U^*(\mathbf{x}, \mathbf{y})$ in Green's second identity

$$\int_K (v(\mathbf{y}) \Delta u(\mathbf{y}) - u(\mathbf{y}) \Delta v(\mathbf{y})) \, \mathrm{d}\mathbf{y} = \int_{\partial K} \left(\gamma_0^K v(\mathbf{y}) \gamma_1^K u(\mathbf{y}) - \gamma_0^K u(\mathbf{y}) \gamma_1^K v(\mathbf{y}) \right) \mathrm{d}s_{\mathbf{y}} \ ,$$

see [128], we obtain a representation formula for the solution u in every point $\mathbf{x} \in K$. It reads

$$u(\mathbf{x}) = \int_{\partial K} U^*(\mathbf{x}, \mathbf{y}) \gamma_1^K u(\mathbf{y}) \, \mathrm{d}s_{\mathbf{y}} - \int_{\partial K} \gamma_{1,\mathbf{y}}^K U^*(\mathbf{x}, \mathbf{y}) \gamma_0^K u(\mathbf{y}) \, \mathrm{d}s_{\mathbf{y}} \ , \tag{4.3}$$

where $\gamma_{1,\mathbf{y}}^K$ denotes the conormal derivative operator with respect to the variable $\mathbf{y}$. By differentiation of (4.3), we obtain formulas for the derivatives of u. Consequently, if the data $\gamma_0^K u$ and $\gamma_1^K u$ is known, it is possible to evaluate the function u and its derivatives everywhere in the domain K. Furthermore, it is possible to compute the Neumann data if the Dirichlet data is known as in (4.1). We apply the trace and the conormal derivative operator to the representation formula and obtain

a system of equations

$$\begin{pmatrix} \gamma_0^K u \\ \gamma_1^K u \end{pmatrix} = \begin{pmatrix} (1-\varsigma)\mathbf{I} - \mathbf{K}_K & \mathbf{V}_K \\ \mathbf{D}_K & \varsigma\mathbf{I} + \mathbf{K}'_K \end{pmatrix} \begin{pmatrix} \gamma_0^K u \\ \gamma_1^K u \end{pmatrix} , \tag{4.4}$$

where

$$\varsigma(\mathbf{x}) = \lim_{\varepsilon \to 0} \frac{1}{2(d-1)\pi} \frac{1}{\varepsilon^{d-1}} \int\limits_{\mathbf{y} \in K : |\mathbf{y}-\mathbf{x}| = \varepsilon} \mathrm{d}s_{\mathbf{y}} \quad \text{for } \mathbf{x} \in \partial K . \tag{4.5}$$

The system (4.4) contains the standard boundary integral operators which are well studied, see, e.g., [128, 151, 159]. For $\mathbf{x} \in \partial K$, we have the single-layer potential operator

$$(\mathbf{V}_K \zeta)(\mathbf{x}) = \gamma_0^K \int_{\partial K} U^*(\mathbf{x}, \mathbf{y}) \zeta(\mathbf{y}) \, \mathrm{d}s_{\mathbf{y}} \quad \text{for } \zeta \in H^{-1/2}(\partial K) ,$$

the double-layer potential operator

$$(\mathbf{K}_K \xi)(\mathbf{x}) = \lim_{\varepsilon \to 0} \int\limits_{\mathbf{y} \in \partial K : |\mathbf{y}-\mathbf{x}| \geq \varepsilon} \gamma_{1,\mathbf{y}}^K U^*(\mathbf{x}, \mathbf{y}) \xi(\mathbf{y}) \, \mathrm{d}s_{\mathbf{y}} \quad \text{for } \xi \in H^{1/2}(\partial K) ,$$

and the adjoint double-layer potential operator

$$(\mathbf{K}'_K \zeta)(\mathbf{x}) = \lim_{\varepsilon \to 0} \int\limits_{\mathbf{y} \in \partial K : |\mathbf{y}-\mathbf{x}| \geq \varepsilon} \gamma_{1,\mathbf{x}}^K U^*(\mathbf{x}, \mathbf{y}) \zeta(\mathbf{y}) \, \mathrm{d}s_{\mathbf{y}} \quad \text{for } \zeta \in H^{-1/2}(\partial K) ,$$

as well as the hypersingular integral operator

$$(\mathbf{D}_K \xi)(\mathbf{x}) = -\gamma_1^K \int_{\partial K} \gamma_{1,\mathbf{y}}^K U^*(\mathbf{x}, \mathbf{y}) \xi(\mathbf{y}) \, \mathrm{d}s_{\mathbf{y}} \quad \text{for } \xi \in H^{1/2}(\partial K) .$$

These integral operators

$$\begin{aligned} \mathbf{V}_K &: H^{-1/2+s}(\partial K) \to H^{1/2+s}(\partial K) , \\ \mathbf{K}_K &: H^{1/2+s}(\partial K) \to H^{1/2+s}(\partial K) , \\ \mathbf{K}'_K &: H^{-1/2+s}(\partial K) \to H^{-1/2+s}(\partial K) , \\ \mathbf{D}_K &: H^{1/2+s}(\partial K) \to H^{-1/2+s}(\partial K) \end{aligned}$$

are linear and continuous for $s \in [-1/2, 1/2]$, see [61, 128]. The system (4.4) can be utilized to derive the following relations between the boundary integral

operators

$$\begin{aligned}
\mathbf{V}_K\mathbf{D}_K &= (\varsigma\mathbf{I}+\mathbf{K})((1-\varsigma)\mathbf{I}-\mathbf{K}_K)\ ,\\
\mathbf{D}_K\mathbf{V}_K &= (\varsigma\mathbf{I}+\mathbf{K}'_K)((1-\varsigma)\mathbf{I}-\mathbf{K}'_K)\ ,\\
\mathbf{V}_K\mathbf{K}'_K &= \mathbf{K}_K\mathbf{V}_K\ ,\\
\mathbf{K}'_K\mathbf{D}_K &= \mathbf{D}_K\mathbf{K}_K\ .
\end{aligned}$$

Remark 4.1 The function $u = 1$ obviously satisfies the Laplace equation and it is $\gamma_0^K u = 1$ and $\gamma_1^K u = 0$. Consequently, we obtain from the first equation in (4.4) that

$$\varsigma(\mathbf{x}) = -\int_{\partial K} \gamma_{1,\mathbf{y}}^K U^*(\mathbf{x},\mathbf{y})\,\mathrm{d}s_{\mathbf{y}} \quad \text{for } \mathbf{x}\in\partial K\ . \tag{4.6}$$

If the boundary ∂K is smooth in a neighbourhood of the point $\mathbf{x}\in\partial K$, i.e., it can be represented locally by a differentiable parametrization, then (4.5) yields

$$\varsigma(\mathbf{x}) = \frac{1}{2}\ .$$

Thus, we have $\varsigma = 1/2$ almost everywhere on ∂K for a polytopal domain K. On the other hand, if $\mathbf{x}\in\partial K$ is on an edge in 3D or it is a vertex, then ς is related to the interior angle of K at the point $\mathbf{x}$. In the two-dimensional case $K\subset\mathbb{R}^2$, it can be shown that

$$\varsigma(\mathbf{x}) = \frac{\alpha}{2\pi}$$

for a corner point $\mathbf{x}$ of a polygonal domain, where $\alpha\in(0,2\pi)$ denotes the interior angle of the polygon at $\mathbf{x}$, see, e.g., [118].

4.2.1 Direct Approach for Dirichlet Problem

For $K\subset\mathbb{R}^2$ with $h_K < 1$ and $K\subset\mathbb{R}^3$, the single-layer potential operator induces a bilinear form $(\mathbf{V}_K\cdot,\cdot)_{L_2(\partial K)}$, which is $H^{-1/2}(\partial K)$-elliptic and continuous on $H^{-1/2}(\partial K)$, see [128, 159]. Here, the L_2-inner product has to be interpreted as duality pairing. According to the Lax–Milgram Lemma the single-layer potential operator is invertible. Therefore, the first equation of system (4.4) yields a relation between the Dirichlet and the Neumann trace, namely

$$\gamma_1^K u = \mathbf{S}_K\gamma_0^K u \quad \text{with} \quad \mathbf{S}_K = \mathbf{V}_K^{-1}\left(\tfrac{1}{2}\mathbf{I}+\mathbf{K}_K\right)\ . \tag{4.7}$$

The operator

$$\mathbf{S}_K : H^{1/2}(\partial K) \to H^{-1/2}(\partial K)$$

is called Steklov–Poincaré operator and (4.7) is its non-symmetric representation. This operator is linear and continuous due to its definition. With the help of the second equation in the system (4.4), we find the symmetric representation

$$\mathbf{S}_K = \mathbf{D}_K + \left(\tfrac{1}{2}\mathbf{I} + \mathbf{K}'_K\right)\mathbf{V}_K^{-1}\left(\tfrac{1}{2}\mathbf{I} + \mathbf{K}_K\right) . \tag{4.8}$$

The inversion of the single-layer potential operator is not desirable in the evaluation of the Steklov–Poincaré operator. In order to compute the unknown Neumann data $t = \gamma_1^K u \in H^{-1/2}(\partial K)$ from given Dirichlet data $g = \gamma_0^K u \in H^{1/2}(\partial K)$, it is more convenient to use the Galerkin formulation

$$\begin{aligned} &\text{Find } t \in H^{-1/2}(\partial K) : \\ &(\mathbf{V}_K t, \zeta)_{L_2(\partial K)} = \left(\left(\tfrac{1}{2}\mathbf{I} + \mathbf{K}_K\right) g, \zeta\right)_{L_2(\partial K)} \qquad \forall \zeta \in H^{-1/2}(\partial K) . \end{aligned} \tag{4.9}$$

This formulation admits a unique solution according to the Lax–Milgram Lemma and is consequently equivalent to the evaluation of $\mathbf{S}_K$. Thus, in order to solve the Dirichlet problem for the Laplace equation (4.1), we may choose the representation formula (4.3) for u and compute its Neumann trace with the help of the Galerkin formulation (4.9). The solution obtained this way satisfies $u \in H^1(K)$, see [128, 159]. This is a direct approach since the Dirichlet and Neumann traces of the unknown solution are either known or computed and used in the representation formula.

4.2.2 *Indirect Approach for Dirichlet Problem*

Alternatively, one may follow an indirect approach. Instead of computing traces of the unknown function, the solution is sought as a potential of an unknown density. It is known, see, e.g., [128, 151, 159], that the double-layer potential

$$u(\mathbf{x}) = \int_{\partial K} \gamma_{1,\mathbf{y}}^K U^*(\mathbf{x}, \mathbf{y}) \xi(\mathbf{y}) \, \mathrm{d}s_{\mathbf{y}} \quad \text{for } \mathbf{x} \in K \tag{4.10}$$

with arbitrary density $\xi \in H^{1/2}(\partial K)$ satisfies the Laplace equation. Thus, the density ξ has to be determined such that the Dirichlet boundary condition in (4.1) is satisfied. Applying the trace operator to (4.10) yields the following boundary integral equation of second kind

$$(1 - \varsigma(\mathbf{x}))\xi(\mathbf{x}) - (\mathbf{K}_K \xi)(\mathbf{x}) = -g(\mathbf{x}) \quad \text{for } \mathbf{x} \in \partial K . \tag{4.11}$$

It admits a unique solution $\xi \in H^{1/2}(\partial K)$ which is formally given as a Neumann series

$$\xi(\mathbf{x}) = -\sum_{\ell=0}^{\infty} (\varsigma \mathbf{I} + \mathbf{K}_K)^{\ell} g(\mathbf{x}) \quad \text{for } \mathbf{x} \in \partial K \ .$$

Furthermore, the series is convergent since $\varsigma \mathbf{I} + \mathbf{K}_K$ is a contraction in $H^{1/2}(\partial K)$, see [160].

4.2.3 Direct Approach for Neumann Problem

Although this chapter focuses on the Dirichlet problem for the Laplace equation, we briefly consider the Neumann problem:

$$-\Delta u = 0 \quad \text{in } K \ , \qquad \gamma_1^K u = t \quad \text{on } \partial K \ ,$$

where $t \in H^{-1/2}(\partial K)$ satisfies the solvability condition

$$\int_{\partial K} t \, \mathrm{d}s_{\mathbf{x}} = 0 \tag{4.12}$$

such that there exists a unique solution

$$u \in H^1_*(K) = \{v \in H^1(K) : (v, 1)_{L_2(\partial K)} = 0\} \ .$$

We follow a direct approach and derive a boundary integral equation for the unknown Dirichlet data $g = \gamma_0^K u \in H^{1/2}(\partial K)$. Afterwards, the representation formula (4.3) gives the solution of the boundary value problem.

In order to find a connection between the Dirichlet and Neumann traces we consider this time the second equation in (4.4), which yields

$$\mathbf{D}_K \gamma_0^K u = \left(\tfrac{1}{2}\mathbf{I} - \mathbf{K}'_K\right) \gamma_1^K u \ . \tag{4.13}$$

The hypersingular integral operator $\mathbf{D}_K$ is self-adjoint and has a non-trivial kernel on $H^{1/2}(\partial K)$, namely it is $\ker \mathbf{D}_K = \operatorname{span}\{1\}$ for a simply connected domain K. Thus, we define the subspace

$$H^{1/2}_*(\partial K) = \{\xi \in H^{1/2}(\partial K) : (\xi, 1)_{L_2(\partial K)} = 0\}$$

of $H^{1/2}(\partial K)$, containing the functions with vanishing mean value, on which $\mathbf{D}_K$ is bounded and elliptic. $H^{1/2}_*(\partial K)$ can be interpreted as trace space of $H^1_*(K)$.

Consequently, (4.13) has a unique solution $\gamma_0^K u$ in $H_*^{1/2}(\partial K)$ for given data $t = \gamma_1^K u$. With a slight abuse of notation, we denote by $\mathbf{D}_K^{-1}$ the inverse of the hypersingular integral operator on the subspace $H_*^{1/2}(\partial K)$, and thus we can write

$$\gamma_0^K u = \mathbf{P}_K \gamma_1^K u \quad \text{with} \quad \mathbf{P}_K = \mathbf{D}_K^{-1} \left(\tfrac{1}{2}\mathbf{I} - \mathbf{K}_K' \right) \tag{4.14}$$

on $H_*^{1/2}(\partial K)$. The operator $\mathbf{P}_K : H^{-1/2}(\partial K) \to H_*^{1/2}(\partial K)$, which maps the Neumann to the Dirichlet data, is called Poincaré–Steklov operator. (Depending on the literature it is sometimes also called Steklov–Poincaré operator.) Employing the properties of the boundary integral operators, the symmetric representation

$$\mathbf{P}_K = \mathbf{V}_K + \left(\tfrac{1}{2}\mathbf{I} - \mathbf{K}_K \right) \mathbf{D}_K^{-1} \left(\tfrac{1}{2}\mathbf{I} - \mathbf{K}_K' \right) \tag{4.15}$$

follows. To compute the unknown Dirichlet data $g = \gamma_0^K u \in H_*^{1/2}(\partial K)$ from given Neumann data $t = \gamma_1^K u \in H^{-1/2}(\partial K)$, we apply a Galerkin formulation once more, namely

$$\begin{aligned} &\text{Find } g \in H_*^{1/2}(\partial K) : \\ &(\mathbf{D}_K g, \xi)_{L_2(\partial K)} = \left((\tfrac{1}{2}\mathbf{I} - \mathbf{K}_K')t, \xi \right)_{L_2(\partial K)} \quad \forall \xi \in H_*^{1/2}(\partial K) \, . \end{aligned} \tag{4.16}$$

This problem is reformulated into a saddle point formulation, which reads

$$\begin{aligned} &\text{Find } (g, \lambda) \in H^{1/2}(\partial K) \times \mathbb{R} : \\ &(\mathbf{D}_K g, \xi)_{L_2(\partial K)} + \lambda(\xi, 1)_{L_2(\partial K)} = \left((\tfrac{1}{2}\mathbf{I} - \mathbf{K}_K')t, \xi \right)_{L_2(\partial K)} \quad \forall \xi \in H^{1/2}(\partial K) \, , \\ &\mu(g, 1)_{L_2(\partial K)} = 0 \quad \forall \mu \in \mathbb{R} \, . \end{aligned}$$

For $g \in H^{1/2}(\partial K) \setminus H_*^{1/2}(\partial K)$, we write $\mu = \lambda/(g, 1)_{L_2(\partial K)} - \alpha$ with $\alpha \in \mathbb{R}$ and obtain from the second equation $\lambda = \alpha(g, 1)_{L_2(\partial K)}$. The expression for the Lagrange multiplier λ also holds for $g \in H_*^{1/2}(\partial K)$, since testing the first equation with $\xi_0 = 1$ yields

$$\lambda(1, 1)_{L_2(\partial K)} = 0$$

and thus $\lambda = 0$. Here, we employed

$$\ker \mathbf{D}_K = \ker \left(\tfrac{1}{2}\mathbf{I} + \mathbf{K}_K \right) = \operatorname{span}\{1\} \, ,$$

$\mathbf{D}_K$ is self-adjoint and the solvability condition (4.12), such that

$$(\mathbf{D}_K g, \xi_0)_{L_2(\partial K)} = (g, \mathbf{D}_K \xi_0)_{L_2(\partial K)} = 0$$

and

$$\left((\tfrac{1}{2}\mathbf{I} - \mathbf{K}'_K)t, \xi_0\right)_{L_2(\partial K)} = (t, \xi_0)_{L_2(\partial K)} - \left(t, (\tfrac{1}{2}\mathbf{I} + \mathbf{K}_K)\xi_0\right)_{L_2(\partial K)} = 0 \,.$$

Inserting $\lambda = \alpha(g, 1)_{L_2(\partial K)}$ into the first equation of the saddle point formulation, we obtain for fixed α the Galerkin formulation:

$$\begin{aligned} &\text{Find } g \in H^{1/2}(\partial K) : \\ &\left(\widetilde{\mathbf{D}}_K g, \xi\right)_{L_2(\partial K)} = \left((\tfrac{1}{2}\mathbf{I} - \mathbf{K}'_K)t, \xi\right)_{L_2(\partial K)} \quad \forall \xi \in H^{1/2}(\partial K) \,, \end{aligned} \tag{4.17}$$

where

$$\left(\widetilde{\mathbf{D}}_K \vartheta, \xi\right)_{L_2(\partial K)} = (\mathbf{D}_K \vartheta, \xi)_{L_2(\partial K)} + \alpha(\vartheta, 1)_{L_2(\partial K)}(\xi, 1)_{L_2(\partial K)} \,.$$

For $\alpha > 0$, the operator $\widetilde{\mathbf{D}}_K$ is bounded and elliptic on $H^{1/2}(\partial K)$ and consequently, the Galerkin formulation has a unique solution $g \in H^{1/2}(\partial K)$. This solution even belongs to $H^{1/2}_*(\partial K)$ since plugging $\xi_0 = 1$ into (4.17) yields with the same arguments as above

$$(g, 1)_{L_2(\partial K)}(1, 1)_{L_2(\partial K)} = 0 \,.$$

Hence, the formulation (4.17) is equivalent to the initial variational formulation and the solution g is independent of α because of the unique solvability.

4.3 Boundary Element Method

The aim of this section is to introduce discrete Galerkin formulations for the direct approaches of the Dirichlet and Neumann problems derived in the previous section. Thus, we discretize the variational formulations (4.9) and (4.17). For this reason, we have to introduce approximation spaces for $H^{1/2}(\partial K)$ and $H^{-1/2}(\partial K)$ as well as in particular a discretization of ∂K. We follow standard approaches as described in [144, 151, 159], for instance.

First, the boundary ∂K of the domain K is decomposed into non-overlapping line segments in two-dimensions and triangles in three-dimensions, see Fig. 4.1, such that the resulting boundary mesh, which is denoted by $\mathscr{B}_h$, is regular. More precisely, we assume that $\mathscr{B}_h$ is shape-regular in the sense of Ciarlet such that neighbouring elements either share a common node or edge and the aspect ratio

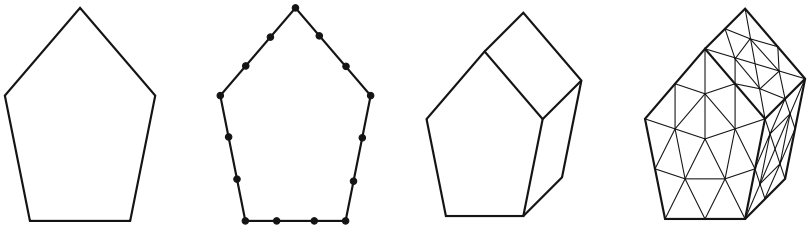

Fig. 4.1 A domain and its boundary mesh for $d = 2$ (left) and $d = 3$ (right)

of each triangle is uniformly bounded. In order to present approximation estimates later on, we additionally assume a uniform boundary mesh in the sense that all elements have comparable size. The elements of the mesh $\mathscr{B}_h$ are denoted by T. For the approximations, we utilize standard spaces of piecewise polynomials. Let $k \in \mathbb{N}$ be the desired approximation order in the boundary element method. We discretize $H^{-1/2}(\partial K)$ and thus the Neumann traces by piecewise polynomials of degree smaller or equal $k-1$ which might be discontinuous over element interfaces. This approximation space is given by

$$\mathscr{P}^{k-1}_{\mathrm{pw,d}}(\mathscr{B}_h) = \left\{ \zeta \in L_2(\partial K) : \zeta\big|_T \in \mathscr{P}^{k-1}(T) \ \forall T \in \mathscr{B}_h \right\} . \tag{4.18}$$

The space $H^{1/2}(\partial K)$ and thus the Dirichlet traces are discretized by piecewise polynomials of degree smaller or equal k which are continuous over element interfaces. This approximation space is given by

$$\mathscr{P}^{k}_{\mathrm{pw}}(\mathscr{B}_h) = \mathscr{P}^{k}_{\mathrm{pw,d}}(\mathscr{B}_h) \cap C^0(\partial K) . \tag{4.19}$$

The choice of spaces yields conforming Galerkin approximations since

$$\mathscr{P}^{k}_{\mathrm{pw}}(\mathscr{B}_h) \subset H^{1/2}(\partial K) \qquad \text{and} \qquad \mathscr{P}^{k-1}_{\mathrm{pw,d}}(\mathscr{B}_h) \subset H^{-1/2}(\partial K) .$$

These spaces are equipped with the usual Lagrangian bases used in finite element methods. In two-dimensions we might also apply the polynomial basis defined in Sect. 2.3.1, cf. Fig. 2.9. The set of basis functions for $\mathscr{P}^{k}_{\mathrm{pw}}(\mathscr{B}_h)$ and $\mathscr{P}^{k-1}_{\mathrm{pw,d}}(\mathscr{B}_h)$ are fixed once and they are denoted in the following by Φ_D and Φ_N, respectively.

4.3.1 Dirichlet Problem

In order to treat the Dirichlet problem (4.1) for the Laplace equation, we utilize the direct approach and approximate the Galerkin formulation (4.9) for the unknown

Neumann trace $t = \gamma_1^K u \in H^{-1/2}(\partial K)$ from Sect. 4.2.1. This yields the discrete Galerkin formulation

$$\begin{aligned} &\text{Find } t_h \in \mathscr{P}^{k-1}_{\mathrm{pw,d}}(\mathscr{B}_h) : \\ &(\mathbf{V}_K t_h, \zeta)_{L_2(\partial K)} = \left(\left(\tfrac{1}{2}\mathbf{I} + \mathbf{K}_K \right) g, \zeta \right)_{L_2(\partial K)} \quad \forall \zeta \in \mathscr{P}^{k-1}_{\mathrm{pw,d}}(\mathscr{B}_h) \,, \end{aligned} \tag{4.20}$$

where g is the given Dirichlet data. Since the bilinear form induced by the single-layer potential operator is $H^{-1/2}(\partial K)$-elliptic as well as continuous on $H^{-1/2}(\partial K)$ and $\mathscr{P}^{k-1}_{\mathrm{pw,d}}(\mathscr{B}_h) \subset H^{-1/2}(\partial K)$, the variational formulation (4.20) admits a unique solution according to the Lax–Milgram Lemma. Furthermore, Céa's Lemma yields

$$\|t - t_h\|_{H^{-1/2}(\partial K)} \leq C \inf_{\zeta \in \mathscr{P}^{k-1}_{\mathrm{pw,d}}(\mathscr{B}_h)} \|t - \zeta\|_{H^{-1/2}(\partial K)} \,.$$

From known approximation properties of polynomials, see [151, Theorem 4.3.20], we obtain

$$\|t - t_h\|_{H^{-1/2}(\partial K)} \leq C\, h^{s+1/2} |t|_{H^s_{\mathrm{pw}}(\partial K)} \,, \tag{4.21}$$

when assuming $t \in H^s_{\mathrm{pw}}(\partial K)$ and $0 \leq s \leq k$. Here, h denotes the mesh size in the boundary element mesh $\mathscr{B}_h$. After the computation of t_h, we utilize it for approximating the solution $u(\mathbf{x})$ of the Dirichlet problem in an interior point $\mathbf{x} \in K$ by the representation formula (4.3). This yields

$$\widetilde{u}(\mathbf{x}) = \int_{\partial K} U^*(\mathbf{x}, \mathbf{y}) t_h(\mathbf{y}) \, \mathrm{d}s_{\mathbf{y}} - \int_{\partial K} \gamma^K_{1,\mathbf{y}} U^*(\mathbf{x}, \mathbf{y}) g(\mathbf{y}) \, \mathrm{d}s_{\mathbf{y}} \,, \tag{4.22}$$

and under the assumption of sufficient regularity we obtain for $k = 1$ the pointwise error estimate

$$|u(\mathbf{x}) - \widetilde{u}(\mathbf{x})| \leq C(\mathbf{x})\, h^3 \, |t|_{H^1_{\mathrm{pw}}(\partial K)} \tag{4.23}$$

for $\mathbf{x} \in K$ and in the $H^1(K)$-norm

$$\|u - \widetilde{u}\|_{H^1(K)} \leq C\, h^{3/2} \, |t|_{H^1_{\mathrm{pw}}(\partial K)} \,.$$

Because of $\mathbf{x} \in K$, the integrands in (4.3) are non-singular and consequently approximation formulas for the derivatives of u can be derived by simply differentiating (4.22). These pointwise approximations of the derivatives converge with the same order as the approximation $\widetilde{u}(\mathbf{x})$ of $u(\mathbf{x})$. We point out, that the integrals in (4.22) can be evaluated analytically for piecewise polynomial data t_h and g. In our later application g is already piecewise polynomial. In the general case, however, the Dirichlet data is approximated by its L_2-projection $g_h \in \mathscr{P}^k_{\mathrm{pw}}(\mathscr{B}_h)$

and the error analysis additionally relies on Strang-type arguments. Utilizing the basis functions in Φ_D and Φ_N for $\mathscr{P}^k_{\mathrm{pw}}(\mathscr{B}_h)$ and $\mathscr{P}^{k-1}_{\mathrm{pw,d}}(\mathscr{B}_h)$, respectively, we make the ansatz

$$g_h(\mathbf{x}) = \sum_{\varphi\in\Phi_D} g_\varphi \varphi(\mathbf{x}) \quad \text{and} \quad t_h(\mathbf{x}) = \sum_{\tau\in\Phi_N} t_\tau \tau(\mathbf{x}) \,, \tag{4.24}$$

where $\mathbf{x} \in \partial K$. Furthermore, we identify the approximations g_h and t_h with their vectors $\underline{g}_h = \left(g_\varphi\right)_{\varphi\in\Phi_D}$ and $\underline{t}_h = (t_\tau)_{\tau\in\Phi_N}$ containing the expansion coefficients. Due to the L_2-projection, the coefficients in $\underline{g}_h$ are given as solution of

$$\sum_{\varphi\in\Phi_D} g_\varphi (\varphi,\xi)_{L_2(\partial K)} = (g,\xi)_{L_2(\partial K)} \quad \forall \xi \in \mathscr{P}^k_{\mathrm{pw}}(\mathscr{B}_h) \,. \tag{4.25}$$

The system of linear equations (4.25) involves the symmetric, positive definite mass matrix

$$\mathbf{M}^{DD}_{K,h} = \left((\varphi,\xi)_{L_2(\partial K)}\right)_{\xi\in\Phi_D,\varphi\in\Phi_D} \,.$$

Inserting the ansatz (4.24) into the discrete Galerkin formulation (4.20) yields a system of linear equations for $\underline{t}_h$, namely

$$\mathbf{V}_{K,h}\underline{t}_h = \left(\tfrac{1}{2}\mathbf{M}_{K,h} + \mathbf{K}_{K,h}\right)\underline{g}_h \,, \tag{4.26}$$

where the matrices are defined as

$$\mathbf{V}_{K,h} = \left((\mathbf{V}_K\tau,\vartheta)_{L_2(\partial K)}\right)_{\vartheta\in\Phi_N,\tau\in\Phi_N}$$

and

$$\mathbf{M}_{K,h} = \left((\varphi,\vartheta)_{L_2(\partial K)}\right)_{\vartheta\in\Phi_N,\varphi\in\Phi_D} \,, \quad \mathbf{K}_{K,h} = \left((\mathbf{K}_K\varphi,\vartheta)_{L_2(\partial K)}\right)_{\vartheta\in\Phi_N,\varphi\in\Phi_D} \,.$$

The system (4.26) is uniquely solvable since the matrix $\mathbf{V}_{K,h}$ is symmetric and positive definite due to the properties of the integral operator $\mathbf{V}_K$.

Remark 4.2 In the computational realization the matrices can be set up in different ways. Either a semi-analytic integration scheme is utilized, which evaluates the boundary integral operators applied to piecewise polynomial functions analytically and approximates the outer integrals by numerical quadrature, or a fully numerical integration scheme is applied. The semi-analytic scheme as well as the analytic formulas are given in [144] and an appropriate fully numerical quadrature is presented in [151] for the three-dimensional case. Corresponding formulas are also available for the two-dimensional case.

The approximation of the Dirichlet to Neumann map with the help of the system of linear equations (4.26) corresponds to the representation (4.7) of the Steklov–Poincaré operator. But, we have also derived a symmetric representation (4.8) which can be utilized to define a symmetric approximation of the Steklov–Poincaré operator. Since the Neumann trace satisfies

$$t = \mathbf{V}_K^{-1} \left(\tfrac{1}{2}\mathbf{I} + \mathbf{K}_K \right) g \ ,$$

we use the previously derived approximation t_h and define

$$\widetilde{\mathbf{S}}_K g = \mathbf{D}_K g + \left(\tfrac{1}{2}\mathbf{I} + \mathbf{K}'_K \right) t_h \ . \tag{4.27}$$

This yields the symmetric discretization of the Steklov–Poincaré operator

$$\mathbf{S}_{K,h} = \mathbf{D}_{K,h} + \left(\tfrac{1}{2}\mathbf{M}_{K,h}^{\top} + \mathbf{K}_{K,h}^{\top} \right) \mathbf{V}_{K,h}^{-1} \left(\tfrac{1}{2}\mathbf{M}_{K,h} + \mathbf{K}_{K,h} \right) \tag{4.28}$$

with the matrix entries

$$\mathbf{S}_{K,h} = \left(\left(\widetilde{\mathbf{S}}_K \varphi, \phi \right)_{L_2(\partial K)} \right)_{\phi \in \Phi_D, \varphi \in \Phi_D} \ ,$$

where

$$\mathbf{D}_{K,h} = \left((\mathbf{D}_K \varphi, \phi)_{L_2(\partial K)} \right)_{\phi \in \Phi_D, \varphi \in \Phi_D} \ .$$

The matrix entries of $\mathbf{D}_{K,h}$ can be assembled with the help of the single-layer potential matrix $\mathbf{V}_{K,h}$. For piecewise smooth functions one can show that

$$(\mathbf{D}_K \varphi, \phi)_{L_2(\partial K)} = (\mathbf{V}_K \operatorname{curl}_{\partial K} \varphi, \operatorname{curl}_{\partial K} \phi)_{L_2(\partial K)} \ ,$$

where $\operatorname{curl}_{\partial K}$ denotes the surface curl of a scalar valued function on ∂K. For more details, we refer the interested reader to [144, 159].

Example 4.3 We demonstrate the performance of the boundary element method and give the numerical orders of convergence, cf. (1.7), for a model problem. Let K be a regular octagon centered at the origin with diameter 0.8, and consider the boundary value problem

$$-\Delta u = 0 \quad \text{in } K \ , \qquad u = g \quad \text{on } \partial K \ ,$$

where the Dirichlet data g is chosen such that the unique solution of the problem is given as $u(\mathbf{x}) = \exp(2\pi(x_1 - 0.3)) \cos(2\pi(x_2 - 0.3))$. The boundary element method is applied on a sequence of meshes for the approximation orders $k = 1, 2, 3$. The first mesh is defined to be the eight sides of the octagon and the following meshes are constructed by subdividing each line segment of the previous mesh

into two new line segments of the same length. In the following tables we distinguish the meshes and the approximation orders by the number of degrees of freedom (DoF) used to approximate the Neumann trace. In Table 4.1, we present the convergence of the Neumann data in the L_2-norm. The observed numerical order of convergence (noc) is k that reflects the theoretical considerations, cf. (4.21). Furthermore, we evaluate the approximation and its gradient with the help of the representation formula (4.22) in the point $(0.2, 0)^\top \in K$ and present the relative errors as well as the numerical orders of convergence in Tables 4.2 and 4.3, respectively. We observe that the pointwise evaluation of the approximation as well as the evaluation of its gradient converge till numerical saturation is reached. For $k = 1$, the pointwise errors converge with cubic order for the function evaluation as well as for the gradient. This coincides with the estimate (4.23). For $k = 2, 3$, the tables indicate numerical convergence orders of 4 and 5, respectively.

Table 4.1 Degrees of freedom (DoF), error $\|t - t_h\|_{L_2(\Omega)}$ (err) and numerical order of convergence (noc) for $k = 1, 2, 3$ in Example 4.3

$k = 1$			$k = 2$			$k = 3$		
DoF	err	noc	DoF	err	noc	DoF	err	noc
8	$3.22 \times 10^{+0}$	–	16	8.06×10^{-1}	–	24	1.53×10^{-1}	–
16	9.90×10^{-1}	1.70	32	2.21×10^{-1}	1.87	48	1.76×10^{-2}	3.13
32	5.37×10^{-1}	0.88	64	5.98×10^{-2}	1.89	96	2.01×10^{-3}	3.12
64	2.63×10^{-1}	1.03	128	1.56×10^{-2}	1.93	192	2.42×10^{-4}	3.05
128	1.29×10^{-1}	1.03	256	3.96×10^{-3}	1.98	384	2.97×10^{-5}	3.03
256	6.40×10^{-2}	1.02	512	9.89×10^{-4}	2.00	768	3.68×10^{-6}	3.02
512	3.18×10^{-2}	1.01	1024	2.47×10^{-4}	2.00	1536	4.57×10^{-7}	3.01
1024	1.59×10^{-2}	1.00	2048	6.17×10^{-5}	2.00	3072	5.70×10^{-8}	3.00
2048	7.92×10^{-3}	1.00	4096	1.54×10^{-5}	2.00	6144	8.01×10^{-9}	2.83
Theory		1			2			3

Table 4.2 Degrees of freedom (DoF), relative error $|u(\mathbf{x}) - \widetilde{u}(\mathbf{x})|/|u(\mathbf{x})|$ for the point evaluation in $\mathbf{x} = (0.2, 0)^\top$ (err) and numerical order of convergence (noc) for $k = 1, 2, 3$ in Example 4.3

$k = 1$			$k = 2$			$k = 3$		
DoF	err	noc	DoF	err	noc	DoF	err	noc
8	3.46×10^{-2}	–	16	2.55×10^{-4}	–	24	1.57×10^{-4}	–
16	9.94×10^{-4}	5.12	32	3.80×10^{-5}	2.75	48	4.45×10^{-6}	5.14
32	1.12×10^{-4}	3.15	64	9.06×10^{-7}	5.39	96	1.19×10^{-7}	5.22
64	1.62×10^{-5}	2.79	128	1.21×10^{-7}	2.91	192	3.02×10^{-9}	5.31
128	2.03×10^{-6}	2.99	256	8.17×10^{-9}	3.89	384	7.46×10^{-11}	5.34
256	2.54×10^{-7}	2.99	512	4.70×10^{-10}	4.12	768	1.83×10^{-12}	5.35
512	3.22×10^{-8}	2.98	1024	2.53×10^{-11}	4.22	1536	3.52×10^{-14}	5.70
1024	4.09×10^{-9}	2.98	2048	1.28×10^{-12}	4.31	3072	4.51×10^{-14}	–
2048	5.20×10^{-10}	2.98	4096	1.69×10^{-13}	2.92	6144	1.21×10^{-13}	–

Table 4.3 Degrees of freedom (DoF), relative error $|\nabla u(\mathbf{x}) - \nabla\widetilde{u}(\mathbf{x})|/|\nabla u(\mathbf{x})|$ for the point evaluation of the gradient in $\mathbf{x} = (0.2, 0)^\top$ (err) and numerical order of convergence (noc) for $k = 1, 2, 3$ in Example 4.3

$k=1$			$k=2$			$k=3$		
DoF	err	noc	DoF	err	noc	DoF	err	noc
8	2.29×10^{-1}	–	16	6.68×10^{-3}	–	24	3.56×10^{-4}	–
16	1.53×10^{-2}	3.90	32	5.64×10^{-5}	6.89	48	2.24×10^{-6}	7.31
32	5.23×10^{-4}	4.87	64	2.09×10^{-6}	4.75	96	5.15×10^{-8}	5.45
64	5.58×10^{-5}	3.23	128	8.13×10^{-8}	4.69	192	1.46×10^{-9}	5.14
128	6.84×10^{-6}	3.03	256	5.14×10^{-9}	3.98	384	3.72×10^{-11}	5.29
256	8.42×10^{-7}	3.02	512	3.06×10^{-10}	4.07	768	9.43×10^{-13}	5.30
512	1.04×10^{-7}	3.01	1024	1.66×10^{-11}	4.20	1536	5.04×10^{-14}	4.22
1024	1.30×10^{-8}	3.01	2048	7.57×10^{-13}	4.46	3072	1.13×10^{-13}	–
2048	1.62×10^{-9}	3.00	4096	7.73×10^{-13}	–	6144	8.21×10^{-13}	–

4.3.2 Neumann Problem

The Neumann problem (4.2.3) is treated along the same lines as the Dirichlet problem in the previous section. We utilize the direct approach and approximate the Galerkin formulation (4.17) for the unknown Dirichlet trace $g = \gamma_0^K u \in H^{1/2}(\partial K)$ from Sect. 4.2.3. This yields the discrete Galerkin formulation

$$\begin{aligned} &\text{Find } g_h \in \mathscr{P}^k_{\mathrm{pw}}(\mathscr{B}_h) : \\ &\left(\widetilde{\mathbf{D}}_K g_h, \xi\right)_{L_2(\partial K)} = \left((\tfrac{1}{2}\mathbf{I} - \mathbf{K}'_K)t, \xi\right)_{L_2(\partial K)} \quad \forall \xi \in \mathscr{P}^k_{\mathrm{pw}}(\mathscr{B}_h) \,, \end{aligned} \tag{4.29}$$

where t is the given Neumann data with $\int_{\partial K} t \, \mathrm{d}s_{\mathbf{x}} = 0$. Since $\widetilde{\mathbf{D}}_K$ is bounded as well as elliptic on $H^{1/2}(\partial K)$ and $\mathscr{P}^k_{\mathrm{pw}}(\mathscr{B}_h) \subset H^{1/2}(\partial K)$, the discrete Galerkin formulation has a unique solution according to the Lax–Milgram Lemma. Furthermore, Céa's Lemma yields

$$\|g - g_h\|_{H^{1/2}(\partial K)} \leq C \inf_{\xi \in \mathscr{P}^k_{\mathrm{pw}}(\mathscr{B}_h)} \|g - \xi\|_{H^{1/2}(\partial K)} \,,$$

where known approximation properties of polynomials, see [151, Theorem 4.3.22], can be applied once more, such that

$$\|g - g_h\|_{H^{1/2}(\partial K)} \leq C \, h^{s-1/2} \|g\|_{H^s(\partial K)} \tag{4.30}$$

for $1/2 \leq s \leq k+1$, when assuming $g \in H^s(\partial K)$. Arguing as in Sect. 4.2.3, we even see that $g_h \in H^{1/2}_*(\partial K)$ since $\xi_0 \in \mathscr{P}^k_{\mathrm{pw}}(\partial K)$. Inserting g_h into the

representation formula (4.3), we obtain for $\mathbf{x} \in K$ the pointwise approximation

$$\widetilde{u}(\mathbf{x}) = \int_{\partial K} U^*(\mathbf{x}, \mathbf{y}) t(\mathbf{y}) \, \mathrm{d}s_{\mathbf{y}} - \int_{\partial K} \gamma_{1,\mathbf{y}}^K U^*(\mathbf{x}, \mathbf{y}) g_h(\mathbf{y}) \, \mathrm{d}s_{\mathbf{y}}$$

for the solution $u(\mathbf{x})$ of the Neumann problem. Under the assumption of sufficient regularity the approximation satisfies for $k = 1$ and $\mathbf{x} \in K$ the error estimate

$$|u(\mathbf{x}) - \widetilde{u}(\mathbf{x})| \leq C(\mathbf{x}) \, h^3 \, |g|_{H^2(\partial K)} \, . \tag{4.31}$$

As in the Dirichlet problem we may approximate the given Neumann trace t by its L_2-projection $t_h \in \mathscr{P}^{k-1}_{\mathrm{pw,d}}(\partial K)$. Utilizing the ansatz (4.24) yields the coefficient vector $\underline{t}_h$ and therefore the approximation t_h as unique solution of

$$\sum_{\tau \in \Phi_N} t_\tau (\tau, \zeta)_{L_2(\partial K)} = (t, \zeta)_{L_2(\partial K)} \quad \forall \zeta \in \mathscr{P}^{k-1}_{\mathrm{pw,d}}(\mathscr{B}_h) \, . \tag{4.32}$$

The system of linear equations (4.32) involves the symmetric, positive definite mass matrix

$$\mathbf{M}_{K,h}^{NN} = \left((\tau, \zeta)_{L_2(\partial K)} \right)_{\zeta \in \Phi_N, \tau \in \Phi_N} \, .$$

The solvability condition $\int_{\partial K} t_h \mathrm{d}s_{\mathbf{x}} = 0$ is retained since $\mathrm{span}\,\{1\} \subset \mathscr{P}^{k-1}_{\mathrm{pw,d}}(\mathscr{B}_h)$. Inserting the ansatz (4.24) into the discrete Galerkin formulation (4.29) yields a system of linear equations for $\underline{g}_h$, namely

$$\widetilde{\mathbf{D}}_{K,h} \underline{g}_h = \left(\tfrac{1}{2} \mathbf{M}_{K,h}^\top - \mathbf{K}_{K,h}^\top \right) \underline{t}_h \, , \tag{4.33}$$

where

$$\widetilde{\mathbf{D}}_{K,h} = \mathbf{D}_{K,h} + \alpha \, \mathbf{d}_{K,h} \, \mathbf{d}_{K,h}^\top \, ,$$

with $\alpha > 0$ and

$$\mathbf{D}_{K,h} = \left((\mathbf{D}_K \varphi, \phi)_{L_2(\partial K)} \right)_{\phi \in \Phi_D, \varphi \in \Phi_D} \, , \quad \mathbf{d}_{K,h} = \left((\varphi, 1)_{L_2(\partial K)} \right)_{\varphi \in \Phi_D} \, .$$

The system (4.33) is uniquely solvable since the matrix $\widetilde{\mathbf{D}}_{K,h}$ is symmetric and positive definite due to the properties of the integral operator $\mathbf{D}_K$.

Example 4.4 We demonstrate the performance of the boundary element method for the Neumann problem. Let K be a regular octagon centered at the origin with diameter 0.8 as in Example 4.3, and consider the boundary value problem

$$-\Delta u = 0 \quad \text{in } K \, , \qquad \gamma_1^K u = t \quad \text{on } \partial K \, ,$$

where the Neumann data t is chosen such that the unique solution of the problem in $H^1_*(K)$ is given as $u(\mathbf{x}) = \exp(2\pi(x_1 - 0.3))\cos(2\pi(x_2 - 0.3)) - C$ with $C \in \mathbb{R}$ such that $(\gamma_1^K u, 1)_{L_2(\partial K)} = 0$. The boundary element method is applied on a sequence of meshes for the approximation orders $k = 1, 2$. The first mesh is defined to be the eight sides of the octagon and the following meshes are constructed by subdividing each line segment of the previous mesh into two new line segments of the same length. In Table 4.4 we give the results for $k = 1$ and in Table 4.5 those for $k = 2$. The meshes are distinguished by the number of degrees of freedom (DoF) used to approximate the Dirichlet trace. From (4.30) we expect that the error $\|g - g_h\|_{L_2(\partial K)}$ of the Dirichlet trace in the L_2-norm converges with order $k+1$. This is verified by the numerical order of convergence (noc) in the tables. For the point evaluation, it has been shown in [159] that for $k = 1$ the optimal error estimate (4.31) is not achieved when the Neumann data has to be approximated

Table 4.4 Degrees of freedom (DoF) and errors $\|g - g_h\|_{L_2(\Omega)}$, $|u(\mathbf{x}) - \widetilde{u}(\mathbf{x})|/|u(\mathbf{x})|$ as well as $|\nabla u(\mathbf{x}) - \nabla\widetilde{u}(\mathbf{x})|/|\nabla u(\mathbf{x})|$ for $\mathbf{x} = (0.2, 0)^\top$ and numerical orders of convergence (noc) for $k = 1$ in Example 4.4

	$\|g - g_h\|_{L_2(\Omega)}$		$\lvert u(\mathbf{x}) - \widetilde{u}(\mathbf{x})\rvert/\lvert u(\mathbf{x})\rvert$		$\lvert\nabla u(\mathbf{x}) - \nabla\widetilde{u}(\mathbf{x})\rvert/\lvert\nabla u(\mathbf{x})\rvert$	
DoF	err	noc	err	noc	err	noc
8	3.23×10^{-1}	–	2.25×10^{-1}	–	1.60×10^{-1}	–
16	7.57×10^{-2}	2.09	4.49×10^{-2}	2.32	3.90×10^{-2}	2.04
32	1.67×10^{-2}	2.18	9.92×10^{-3}	2.18	8.97×10^{-3}	2.12
64	3.85×10^{-3}	2.12	2.41×10^{-3}	2.04	2.21×10^{-3}	2.02
128	9.19×10^{-4}	2.07	5.98×10^{-4}	2.01	5.51×10^{-4}	2.01
256	2.24×10^{-4}	2.04	1.49×10^{-4}	2.01	1.38×10^{-4}	2.00
512	5.52×10^{-5}	2.02	3.71×10^{-5}	2.00	3.44×10^{-5}	2.00
1024	1.37×10^{-5}	2.01	9.28×10^{-6}	2.00	8.59×10^{-6}	2.00
2048	3.41×10^{-6}	2.01	2.32×10^{-6}	2.00	2.15×10^{-6}	2.00

Table 4.5 Degrees of freedom (DoF) and errors $\|g - g_h\|_{L_2(\Omega)}$, $|u(\mathbf{x}) - \widetilde{u}(\mathbf{x})|/|u(\mathbf{x})|$ as well as $|\nabla u(\mathbf{x}) - \nabla\widetilde{u}(\mathbf{x})|/|\nabla u(\mathbf{x})|$ for $\mathbf{x} = (0.2, 0)^\top$ and numerical orders of convergence (noc) for $k = 2$ in Example 4.4

	$\|g - g_h\|_{L_2(\Omega)}$		$\lvert u(\mathbf{x}) - \widetilde{u}(\mathbf{x})\rvert/\lvert u(\mathbf{x})\rvert$		$\lvert\nabla u(\mathbf{x}) - \nabla\widetilde{u}(\mathbf{x})\rvert/\lvert\nabla u(\mathbf{x})\rvert$	
DoF	err	noc	err	noc	err	noc
16	3.46×10^{-2}	–	2.57×10^{-3}	–	2.45×10^{-2}	–
32	4.52×10^{-3}	2.94	4.88×10^{-4}	2.40	5.24×10^{-4}	5.55
64	6.06×10^{-4}	2.90	9.06×10^{-5}	2.43	2.06×10^{-5}	4.67
128	8.02×10^{-5}	2.92	2.18×10^{-5}	2.06	9.46×10^{-7}	4.45
256	1.04×10^{-5}	2.95	5.61×10^{-6}	1.96	5.56×10^{-8}	4.09
512	1.34×10^{-6}	2.95	1.44×10^{-6}	1.96	4.15×10^{-9}	3.74
1024	1.79×10^{-7}	2.91	3.65×10^{-7}	1.98	3.16×10^{-10}	3.72
2048	2.66×10^{-8}	2.75	8.99×10^{-8}	2.02	2.30×10^{-11}	3.78
4096	4.58×10^{-9}	2.54	2.04×10^{-8}	2.14	8.61×10^{-13}	4.74

by (4.32). Instead, only

$$|u(\mathbf{x}) - \widetilde{u}(\mathbf{x})| \leq C(\mathbf{x})\, h^2\, |g|_{H^2(\partial K)}$$

is obtained. This theoretical result is confirmed in Table 4.4. Furthermore, the quadratic convergence also holds for $k = 2$ in the numerical experiment, see Table 4.5. For the pointwise convergence of the gradient, the tables indicate numerical convergence orders of 2 and 4 for $k = 1$ and $k = 2$, respectively.

4.4 Nyström Approach

The Nyström method is an alternative approach for the approximation of integral equations. It was initially designed for domains with globally parametrized and smooth boundaries and was later adapted to domains with corners. Here, we restrict ourselves to the two-dimensional case and we utilize the indirect approach for the Dirichlet problem discussed in Sect. 4.2.2. The main idea is to replace the integral by a suitable quadrature formula and to approximate the resulting equation by means of collocation.

First of all, we seek the solution of the Laplace equation in the form (4.10) such that the unknown density ξ has to be approximated. In the case of the two-dimensional Laplace equation we have

$$\gamma_{1,\mathbf{y}}^K U^*(\mathbf{x}, \mathbf{y}) = \frac{(\mathbf{x} - \mathbf{y}) \cdot \mathbf{n}_K(\mathbf{y})}{2\pi\, |\mathbf{x} - \mathbf{y}|^2} \tag{4.34}$$

almost everywhere, where $\mathbf{n}_K(\mathbf{y})$ denotes the outer normal vector of K in the boundary point $\mathbf{y} \in \partial K$. The density ξ satisfies the boundary integral equation (4.11).

4.4.1 Domains with Smooth Boundary

If the boundary of the domain is smooth, i.e. C^2, and there is a global parametrization $\mathbf{x}(\theta)$ such that

$$\partial K = \left\{ \mathbf{x}(\theta) \in \mathbb{R}^2 : \theta_0 \leq \theta \leq \theta_1 \right\}$$

with $|\mathbf{x}'(\theta)| \neq 0$ for all $\theta \in [\theta_0, \theta_1]$, then (4.34) holds for all $\mathbf{x}, \mathbf{y} \in \partial K$ with a removable singularity at $\mathbf{x} = \mathbf{y}$. Furthermore, let the parametric curve be given as $\mathbf{x}(\theta) = (x_1(\theta), x_2(\theta))^\top$ in counter-clockwise orientation. Hence, the outer normal vector can be expressed as $\mathbf{n}_K(\mathbf{x}(\theta)) = (x_2'(\theta), -x_1'(\theta))^\top / |\mathbf{x}'(\theta)|$. Respecting

Remark 4.1, the integral equation (4.11) for the density ξ now reads

$$\tfrac{1}{2}\xi(\mathbf{x}(\theta))+\int_{\theta_0}^{\theta_1}\kappa(\mathbf{x}(\theta),\mathbf{x}(\tau))\xi(\mathbf{x}(\tau))\,\mathrm{d}\tau = -g(\mathbf{x}(\theta)) \quad \text{for } \theta\in[\theta_0,\theta_1]\,, \tag{4.35}$$

with the integral kernel

$$\kappa(\mathbf{x}(\theta),\mathbf{x}(\tau)) = \begin{cases} \dfrac{1}{2\pi}\dfrac{x_1'(\tau)(x_2(\theta)-x_2(\tau))-x_2'(\tau)(x_1(\theta)-x_1(\tau))}{(x_1(\theta)-x_1(\tau))^2+(x_2(\theta)-x_2(\tau))^2}\,, & \text{for } \theta\neq\tau\,, \\ \dfrac{1}{4\pi}\dfrac{x_1'(\tau)x_2''(\tau)-x_2'(\tau)x_1''(\tau)}{(x_1'(\tau))^2+(x_2'(\tau))^2}\,, & \text{for } \theta=\tau\,. \end{cases}$$

Next, we apply the composite trapezoidal rule to the integral with $N+1$ uniformly placed quadrature points $\mathbf{x}_j$, $j=0,\ldots,N$ and weights. Since ξ is periodic on the closed boundary, this quadrature rule is especially suited for the integration, see [62]. Furthermore, we have $\xi(\mathbf{x}_N)=\xi(\mathbf{x}_0)$. The resulting equation cannot hold for all $\theta\in[\theta_0,\theta_1]$ and therefore we enforce its validity by collocation in the quadrature notes. Consequently, we find due to the periodicity the following system of linear equations for the unknown values $\xi_i=\xi(\mathbf{x}_i)$ of the density:

$$\tfrac{1}{2}\xi_i+\sum_{j=1}^{N}\kappa(\mathbf{x}_i,\mathbf{x}_j)\xi_j\omega_j = -g(\mathbf{x}_i) \quad \text{for } i=1,\ldots,N\,, \tag{4.36}$$

where the quadrature points and weights are given by

$$\mathbf{x}_j=\mathbf{x}\left(\theta_0+j\frac{\theta_1-\theta_0}{N}\right) \qquad \text{and} \qquad \omega_j=\frac{\theta_1-\theta_0}{N}\,.$$

It is known that this trapezoidal Nyström method converges with order $\mathcal{O}(1/N^q)$ in the maximum norm, where $q\geq 0$ is related to the smoothness of the boundary ∂K as well as to the smoothness of ξ, see, e.g. [118]. Having the values ξ_i at hand we can approximate $u(\mathbf{x})$ for $\mathbf{x}\in K$ with the help of (4.10) and the trapezoidal rule by

$$\widetilde{u}(\mathbf{x}) = -\sum_{j=1}^{N}\kappa(\mathbf{x},\mathbf{x}_j)\xi_j\omega_j \quad \text{for } \mathbf{x}\in K\,. \tag{4.37}$$

Since the integrand in (4.10) is smooth for $\mathbf{x}\in K$, differentiation and integration can be interchanged. Thus, we obtain an approximation of the gradient of the solution $\nabla u(\mathbf{x})$ as

$$\nabla\widetilde{u}(\mathbf{x}) = -\sum_{j=1}^{N}\nabla\kappa(\mathbf{x},\mathbf{x}_j)\xi_j\omega_j \quad \text{for } \mathbf{x}\in K\,. \tag{4.38}$$

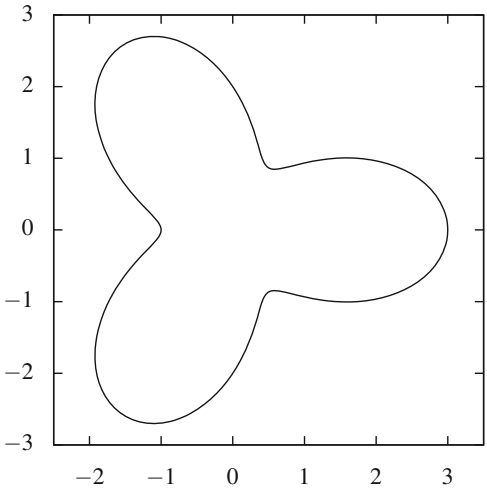

Fig. 4.2 Domain in Example 4.5 which is given by a globally smooth curve describing its boundary

The gradient of the integral kernel can be computed analytically by a small exercise and does not involve any difficulties.

Example 4.5 We consider the boundary value problem

$$-\Delta u = 0 \quad \text{in } K\ , \qquad u = g \quad \text{on } \partial K\ ,$$

where g is chosen such that $u(\mathbf{x}) = \ln|\mathbf{x} - \mathbf{x}^*|$ with $\mathbf{x}^* = (3,3)^\top \notin K$ is the exact solution. The domain K is given by its boundary that is defined as a globally smooth curve with parametrization

$$\mathbf{x}(\theta) = (2 + \cos(3\theta)) \begin{pmatrix} \cos(\theta) \\ \sin(\theta) \end{pmatrix} \quad \text{for} \quad 0 \le \theta < 2\pi\ ,$$

see Fig. 4.2. In Table 4.6, the convergence of the approximation (4.37) as well as of its gradient (4.38) is presented in the point $(1.5, 0)^\top$ for an increasing number of quadrature points (QP) which is equal N in this setting. Furthermore, the numerical order of convergence (noc) is given with respect to $1/N$. Obviously, the Nyström approach converges very fast till machine precision for domains with smooth boundaries.

4.4.2 Domains with Corners

Often, boundary value problems are considered on domains whose boundaries are not given as a globally smooth parametric curves and which may contain corners.

Table 4.6 Number of quadrature points (QP = N), pointwise error of approximation and its gradient in the point $\mathbf{x} = (1.5, 0)^\top$ as well as numerical order of convergence (noc) for Example 4.5

QP	$\lvert u(\mathbf{x}) - \widetilde{u}(\mathbf{x})\rvert / \lvert u(\mathbf{x})\rvert$	noc	$\lvert \nabla u(\mathbf{x}) - \nabla \widetilde{u}(\mathbf{x})\rvert / \lvert \nabla u(\mathbf{x})\rvert$	noc
4	5.12×10^{-1}	–	$1.59 \times 10^{+0}$	–
8	1.71×10^{-1}	1.58	$2.47 \times 10^{+0}$	−0.64
16	6.80×10^{-3}	4.65	1.86×10^{-1}	3.73
32	1.92×10^{-5}	8.47	1.64×10^{-3}	6.83
64	2.69×10^{-8}	9.48	2.38×10^{-7}	12.75
128	5.80×10^{-14}	18.82	4.12×10^{-13}	19.14
256	1.83×10^{-16}	8.31	5.27×10^{-16}	9.61

Consequently, we consider domains with piecewise smooth boundaries next. Thus, the boundary ∂K is decomposed into boundary segments such that each can be parametrized by a smooth curve. Without loss of generality, we concatenate these parametrizations to a piecewise smooth and globally given parametrization which is oriented counter-clockwise. Therefore, let $M \in \mathbb{N}$ be the number of boundary segments, we write

$$\partial K = \left\{ \mathbf{x}(\theta) \in \mathbb{R}^2 : \theta_\ell \le \theta \le \theta_{\ell+1}, \ell = 0, \dots, M-1 \right\} .$$

Here, $|\mathbf{x}'(\theta)| \neq 0$ for all $\theta \in (\theta_\ell, \theta_{\ell+1})$, $\ell = 0, \dots, M-1$ and $\mathbf{z}_\ell = \mathbf{x}(\theta_\ell)$ are the corner points or vertices of the domain. Since the boundary is closed we obviously have $\mathbf{x}(\theta_0) = \mathbf{x}(\theta_M)$. A special case are the polygonal domains which are used throughout this book. In this situation the boundary segments are given as straight lines and $\mathbf{x}'(\theta)$ is constant on each interval $(\theta_\ell, \theta_{\ell+1})$. Furthermore, the vertices $\mathbf{z}_\ell$ coincide with the nodes of the polygonal elements.

In order to derive the Nyström approximation we consider once more the boundary integral equation (4.11). But, since the boundary of the domain is not smooth in the points $\mathbf{z}_\ell$, we have to take care on $\varsigma(\mathbf{z}_\ell)$ which depends on the interior angle of the domain. This dependency is resolved by using (4.6) and reformulating (4.11) to

$$\frac{\xi(\mathbf{x}) + \xi(\mathbf{z})}{2} - \int_{\partial K} \gamma_{1,y}^K U^*(\mathbf{x}, \mathbf{y})(\xi(\mathbf{y}) - \xi(\mathbf{z}))\, \mathrm{d}s_{\mathbf{y}} = -g(\mathbf{x}) \quad \text{for } \mathbf{x} \in \partial K ,$$

where $\mathbf{z}$ is the closest vertex $\mathbf{z}_\ell$ to $\mathbf{x}$. Next, the boundary integral is split into its contributions over the single boundary segments. The parametrization and the outer normal vector are treated within each smooth segment as in the previous section. This yields

$$\frac{\xi(\mathbf{x}(\theta)) + \xi(\mathbf{z})}{2} + \sum_{\ell=0}^{M-1} \int_{\theta_\ell}^{\theta_{\ell+1}} \kappa(\mathbf{x}(\theta), \mathbf{x}(\tau))(\xi(\mathbf{x}(\tau)) - \xi(\mathbf{z}))\, \mathrm{d}\tau = -g(\mathbf{x}(\theta))$$

for $\theta \in [\theta_0, \theta_M]$. If $\theta = \theta_\ell$, $\ell = 0, \ldots, M$, i.e. $\mathbf{x}(\theta) = \mathbf{z}_\ell$, there is a singularity in the integral kernel and the formula of the previous section for $\kappa(\mathbf{z}_\ell, \mathbf{z}_\ell)$ is actually not well defined. Instead of applying the composite trapezoidal rule directly, Kress proposed to perform a sigmoidal change-of-variables first, which copes with the singularity, see [117]. This variable transformation $\eta^{(\ell)} : [0, 1] \to [\theta_\ell, \theta_{\ell+1}]$ is strictly monotonic increasing and it is defined by

$$\eta^{(\ell)}(t) = \theta_\ell + \frac{\big(c(t)\big)^p (\theta_{\ell+1} - \theta_\ell)}{\big(c(t)\big)^p + \big(1 - c(t)\big)^p} ,$$

where $c : [0, 1] \to [0, 1]$ with

$$c(t) = \left(\frac{1}{2} - \frac{1}{p}\right)(2t - 1)^3 + \frac{1}{p}(2t - 1) + \frac{1}{2}$$

and $p \geq 2$ is an integer. It is straight-forward to see that $\big(\eta^{(\ell)}\big)'$ has a root of order $p-1$ at each endpoint of the interval $[0, 1]$. Thus, we obtain with sufficiently large p and the composite trapezoidal rule on each boundary segment

$$\int_{\theta_\ell}^{\theta_{\ell+1}} \kappa(\mathbf{x}(\theta), \mathbf{x}(\tau))(\xi(\mathbf{x}(\tau)) - \xi(\mathbf{z}))\, \mathrm{d}\tau \approx \sum_{j=1}^{N-1} \kappa\big(\mathbf{x}(\theta), \mathbf{x}_j^{(\ell)}\big) \Big(\xi\big(\mathbf{x}_j^{(\ell)}\big) - \xi(\mathbf{z})\Big)\, \omega_j^{(\ell)}$$

where the quadrature points and weights are given by

$$\mathbf{x}_j^{(\ell)} = \mathbf{x}\Big(\eta^{(\ell)}(j/N)\Big) \qquad \text{and} \qquad \omega_j^{(\ell)} = \frac{\big(\eta^{(\ell)}\big)'(j/N)}{N} ,$$

$j = 0, \ldots, N$. The summands for $j = 0, N$ vanish because of the roots of $\big(\eta^{(\ell)}\big)'$. A careful convergence analysis of this quadrature is given in [117], showing that it is convergent for the kinds of integrands we encounter here of increasingly higher order in N as p is increased.

Applying the sigmoidal transform and the trapezoidal rule as above to the modified boundary integral equation and using collocation in the quadrature points yields the following system of linear equations with unknowns $\xi_i^{(k)} = \xi(\mathbf{x}_i^{(k)})$:

$$\frac{\xi_i^{(k)} + \tilde{\xi}_i^{(k)}}{2} + \sum_{\ell=0}^{M-1} \sum_{j=1}^{N-1} \kappa\big(\mathbf{x}_i^{(k)}, \mathbf{x}_j^{(\ell)}\big) \Big(\xi_j^{(\ell)} - \tilde{\xi}_i^{(k)}\Big)\, \omega_j^{(\ell)} = -g\big(\mathbf{x}_i^{(k)}\big) \tag{4.39}$$

for $i = 0, \ldots, N-1$, $k = 0, \ldots, M-1$, where $\tilde{\xi}_i^{(k)}$ is either $\xi_0^{(k)}$ or $\xi_N^{(k)}$ depending which point $\mathbf{x}_0^{(k)}$ or $\mathbf{x}_N^{(k)}$ is closer to $\mathbf{x}_i^{(k)}$. After we have solved the system, the function value $u(\mathbf{x})$ can be approximated for $\mathbf{x} \in K$ with the help of (4.10) and

the quadrature by

$$\widetilde{u}(\mathbf{x}) = -\sum_{\ell=0}^{M-1}\sum_{j=1}^{N} \kappa\big(\mathbf{x}, \mathbf{x}_j^{(\ell)}\big)\xi_j^{(\ell)}\omega_j^{(\ell)} \quad \text{for } \mathbf{x} \in K \ . \tag{4.40}$$

Analogously, we obtain for the gradient $\nabla u(\mathbf{x})$ the approximation

$$\nabla\widetilde{u}(\mathbf{x}) = -\sum_{\ell=0}^{M-1}\sum_{j=1}^{N} \nabla\kappa\big(\mathbf{x}, \mathbf{x}_j^{(\ell)}\big)\xi_j^{(\ell)}\omega_j^{(\ell)} \quad \text{for } \mathbf{x} \in K \ . \tag{4.41}$$

Example 4.6 We consider the boundary value problem

$$-\Delta u = 0 \quad \text{in } K \ , \qquad u = g \quad \text{on } \partial K \ ,$$

where g is chosen such that $u(\mathbf{x}) = \ln|\mathbf{x} - \mathbf{x}^*|$ with $\mathbf{x}^* = (6, 8)^\top \notin K$ is the exact solution. The domain K is given by its boundary that is defined globally as a curve which is piecewise smooth. More precisely, we use the parametrization of an epicycloid that is

$$\mathbf{x}(\theta) = \begin{pmatrix} 8\cos(\theta) - \cos(8\theta) \\ 8\sin(\theta) - \sin(8\theta) \end{pmatrix} \quad \text{for} \quad 0 \le \theta < 2\pi \ ,$$

with corners for $\theta = \theta_\ell = 2\pi\ell/7$, $\ell = 0, \ldots, 7$, see Fig. 4.3. The Nyström approach is applied with the parameter $p = 4$ in the sigmoidal change-of-variable. Each of the $M = 7$ smooth parts of the boundary is decomposed into N segments and thus $N + 1$ quadrature points. In Table 4.7, the convergence of the approximation (4.40)

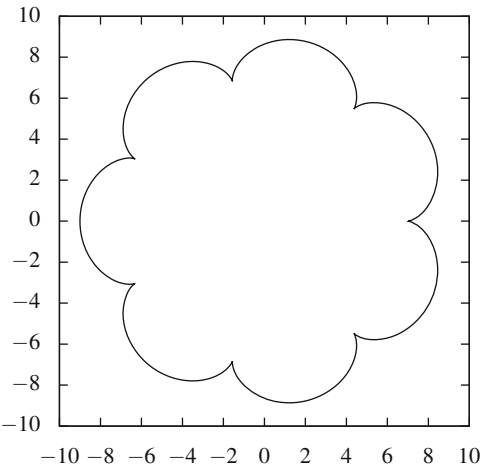

Fig. 4.3 Domain in Example 4.6 with piecewise smooth boundary which is given as parametrization of an epicycloid

Table 4.7 Number of quadrature points (QP= MN), pointwise error of approximation and its gradient in the point $\mathbf{x} = (5.6, 0)^\top$ as well as numerical order of convergence (noc) for Example 4.6 with parameter $p = 4$

QP	$\lvert u(\mathbf{x}) - \widetilde{u}(\mathbf{x})\rvert/\lvert u(\mathbf{x})\rvert$	noc	$\lvert \nabla u(\mathbf{x}) - \nabla\widetilde{u}(\mathbf{x})\rvert/\lvert \nabla u(\mathbf{x})\rvert$	noc
28	3.79×10^{-2}	–	3.41×10^{-1}	–
56	7.18×10^{-5}	9.04	3.19×10^{-2}	3.42
112	9.03×10^{-6}	2.99	6.54×10^{-5}	8.93
224	8.00×10^{-10}	13.46	2.26×10^{-7}	8.18
448	1.73×10^{-12}	8.85	6.89×10^{-10}	8.36
896	1.28×10^{-15}	10.40	3.43×10^{-13}	10.97
1792	8.54×10^{-16}	0.58	1.36×10^{-15}	7.98

as well as of its gradient (4.41) is presented in the point $(5.6, 0)^\top$ for an increasing number of quadrature points (QP) which is equal MN in total. Furthermore, the numerical order of convergence (noc) is given with respect to $1/\text{QP}$. Obviously, the Nyström approach also converges very fast till machine precision for domains with piecewise smooth boundaries when the singularities at the corners are treated with an appropriate quadrature scheme.

4.5 Application in BEM-Based FEM

Throughout this book all numerical experiments and test have been performed with the help of a local BEM solver as described in the following. However, we also give a brute-force application of a local Nyström solver and discuss its potential advantageous and disadvantageous in the next sections for a test problem.

4.5.1 Incorporation of Local Solvers and Quadrature on Polytopes

Before we discuss details of the realization of the BEM-based FEM and the incorporation of the local BEM and Nyström solvers, we recapitulate the problem setting. An isotropic diffusion equation with mixed boundary data and a non-vanishing source term is considered as model problem (2.1) on a domain $\Omega \subset \mathbb{R}^d$, $d = 2, 3$ with boundary $\Gamma = \Gamma_D \cup \Gamma_N$. The domain Ω is decomposed into polytopal elements and the discrete Galerkin formulation (2.28) reads:

$$\text{Find } u_h \in g_D + V_{h,D}^k :$$
$$b(u_h, v_h) = (f, v_h)_{L_2(\Omega)} + (g_N, v_h)_{L_2(\Gamma_N)} \quad \forall v_h \in V_{h,D}^k ,$$

where $b(u_h, v_h) = (a\nabla u_h, \nabla v_h)_{L_2(\Omega)}$, and the approximation space admits the decomposition $V_{h,D}^k = V_{h,H,D}^k \oplus V_{h,B}^k$ into two types of functions. The first ones are harmonic on each element and have piecewise polynomial data on the skeleton of the discretization, whereas the second ones vanish on the skeleton and have a polynomial Laplacian on each element. In particular, the discrete Galerkin formulation decouples for these kinds of functions as given in (2.31) and (2.32) in the case of a piecewise constant diffusion coefficient.

It remains to discuss the realization of the different terms in the discrete Galerkin formulation with the help of the local boundary element method and the local Nyström solver from this chapter. First of all, we recognize that every function $v_h \in V_{h,D}^k$ is given uniquely over each element $K \in \mathscr{K}_h$ by the local boundary value problem

$$-\Delta v_h = p_K \quad \text{in } K \quad \text{and} \quad v_h = p_{\partial K} \quad \text{on } \partial K$$

with prescribed data $p_K \in \mathscr{P}^{k-2}(K)$ and $p_{\partial K} \in \mathscr{P}_{\mathrm{pw}}^k(\partial K)$, cf. (2.14) and (2.15). Since p_K is a polynomial, we can write $v_h = v_{h,H} + q$ with $q \in \mathscr{P}^k(K)$ such that

$$-\Delta v_{h,H} = 0 \quad \text{in } K \quad \text{and} \quad v_{h,H} = p_{\partial K} - q \quad \text{on } \partial K \tag{4.42}$$

with $p_{\partial K} - q \in \mathscr{P}_{\mathrm{pw}}^k(\partial K)$. Therefore, it was sufficient to consider the pure Laplace problem in the previous sections for the local solvers. A constructive approach for finding q is presented in [113]. For a homogeneous polynomial $p \in \mathscr{P}^m(\mathbb{R}^d)$ of degree m, i.e. $p(c\mathbf{x}) = c^m p(\mathbf{x})$, the polynomial

$$q(\mathbf{x}) = \sum_{\ell=0}^{\lfloor m/2 \rfloor} \frac{(-1)^\ell \Gamma(d/2 + m - \ell)}{\Gamma(d/2 + m + 1)(\ell + 1)!} \left(\frac{|\mathbf{x}|^2}{4} \right)^{\ell+1} \Delta^\ell p(\mathbf{x}) \in \mathscr{P}^{m+2}(K)$$

satisfies $\Delta q = p$, where $\lfloor m/2 \rfloor$ denotes the integer part of $m/2$ and $\Gamma(\cdot)$ the gamma function, see [113, Theorem 2]. For non-homogeneous polynomials p the construction can be applied on the representation of p in the monomial basis, whose basis functions are homogeneous.

Let us focus on the two terms $(f, v_h)_{L_2(\Omega)}$ and $(g_N, v_h)_{L_2(\Gamma_N)}$. The latter one does not cause any difficulties. The Neumann boundary Γ_N is given as collection of line segments ($d = 2$) or triangles ($d = 3$) and the restrictions of the functions $v_h \in V_{h,D}^k$ onto Γ_N are piecewise polynomials. Consequently, we apply Gaussian quadrature on each segment or standard numerical integration on each triangle in order to approximate the integral value of the product of the given Neumann data g_N and the piecewise polynomial data of v_h over Γ_N. We also have to apply a quadrature scheme to approximate $(f, v_h)_{L_2(\Omega)}$ since no additional information on f is given in general. For this reason, we decompose the integral first into its contribution over the elements $K \in \mathscr{K}_h$ and afterwards we decompose it even further to its contributions over the triangles ($d = 2$) and tetrahedra ($d = 3$) of the auxiliary

triangulation $\mathscr{T}_h(K)$, i.e.

$$(f, v_h)_{L_2(\Omega)} = \sum_{K \in \mathscr{K}_h} (f, v_h)_{L_2(K)} = \sum_{K \in \mathscr{K}_h} \sum_{T \in \mathscr{T}_h(K)} (f, v_h)_{L_2(T)} \,. \tag{4.43}$$

Now, we apply Gaussian quadrature over each triangle/tetrahedron T. Instead of utilizing the auxiliary discretization $\mathscr{T}_h(K)$ introduces in Sect. 2.2, we may also triangulate the elements with some software tool like `triangle` or `TetGen`, see [155, 157]. This strategy has been especially performed in the numerical tests in order to compute accurate errors in the L_2- and H^1-norm. The evaluation of v_h inside the elements is realized by means of the reformulation $v_h = v_{h,H} + q$ with (4.42) and the approximated representation formulas (4.22) and (4.40), respectively. This natural idea to apply a quadrature rule over a subtriangulation in order to approximate an integral over a polygonal domain has been applied in [164] for instance. An alternative approach is presented in [131], where quadrature points and weights for fixed polygonal domains are precomputed.

In order to treat the bilinear form we have different possibilities. We assume here that the diffusion coefficient is constant on each element and we split the integral into its contributions over the single elements

$$b(u_h, v_h) = (a\nabla u_h, \nabla v_h)_{L_2(\Omega)} = \sum_{K \in \mathscr{K}_h} a_K (\nabla u_h, \nabla v_h)_{L_2(K)} \,.$$

A brute-force approach would be to approximate the term $(\nabla u_h, \nabla v_h)_{L_2(K)}$ by a quadrature as described above using the representation formulas for the evaluation of ∇u_h and ∇v_h in the quadrature points. Alternatively, we may use Green's first identity (4.2) on each element such that

$$(\nabla u_h, \nabla v_h)_{L_2(K)} = (\gamma_1^K u_h, \gamma_0^K v_h)_{L_2(\partial K)} - (\Delta u_h, v_h)_{L_2(K)} \,.$$

Obviously, if either u_h or v_h is harmonic, the volume integral vanishes and we end up with a boundary integral solely, where the product of a Dirichlet and a Neumann trace has to be integrated. Since the approximation space $V_{h,D}^k = V_{h,H,D}^k \oplus V_{h,B}^k$ is given as a direct sum, we distinguish three cases:

1. $u_h, v_h \in V_{h,H,D}^k$: We end up with solely boundary integrals

$$(\nabla u_h, \nabla v_h)_{L_2(K)} = (\gamma_1^K u_h, \gamma_0^K v_h)_{L_2(\partial K)} \,.$$

2. $u_h, v_h \in V_{h,B}^k$: Let $v_h = v_{h,H} + q$ with (4.42), where $p_{\partial K} = 0$, then

$$(\nabla u_h, \nabla v_h)_{L_2(K)} = -(\Delta u_h, v_h)_{L_2(K)} = (\gamma_1^K u_h, \gamma_0^K v_{h,H})_{L_2(\partial K)} - (\Delta u_h, q)_{L_2(K)} \,.$$

3. $u_h \in V_{h,H,D}^k$, $v_h \in V_{h,B}^k$ or vice versa: As we have seen in (2.30), it is

$$(\nabla u_h, \nabla v_h)_{L_2(K)} = 0 \,.$$

The only volume integral which is left is $(\Delta u_h, v_h)_{L_2(K)}$. Since $\Delta u_h \in \mathscr{P}^{k-2}(K)$, the integrand is a polynomial of degree smaller or equal $2k-2$. The integral can thus be computed exactly by the quadrature over the auxiliary discretization or alternatively by applying the divergence theorem followed by a quadrature over the boundary of the element.

Local BEM Solver

The local BEM solver, which is used throughout this book, makes use of the reformulation of the bilinear form in order to reduce the volume integrals to integrals over the skeleton of the domain. More precisely, we end up with integrals over the element boundaries, where we have to integrate the product of a Dirichlet and Neumann trace of functions in V_h^k. This setting nicely fits into the boundary element strategy. The Dirichlet trace of the functions is known whereas their Neumann trace have to be approximated. Here, we proceed as described in Sect. 4.3.

Let $K \in \mathscr{K}_h$ and $\mathscr{B}_h$ be an appropriate boundary element mesh of ∂K consisting of line segments ($d=2$) or triangles ($d=3$). Furthermore, we denote by Φ_D and Φ_N the basis of $\mathscr{P}^k_{\mathrm{pw}}(\mathscr{B}_h)$ and $\mathscr{P}^{k-1}_{\mathrm{pw,d}}(\mathscr{B}_h)$, which are used as approximation spaces for $H^{1/2}(\partial K)$ and $H^{-1/2}(\partial K)$, respectively. Since $\gamma_0^K u_h$ is already polynomial of degree k over each edge/face of K, the trace is represented exactly in the basis Φ_D such that in the notation of Sect. 4.3 it is $g_h^{(u)} = \gamma_0^K u_h \in \mathscr{P}^k_{\mathrm{pw}}(\mathscr{B}_h)$. The Neumann trace $\gamma_1^K u_h$ is approximated by $t_h^{(u)} \in \mathscr{P}^{k-1}_{\mathrm{pw,d}}(\mathscr{B}_h)$ according to the discrete Galerkin formulation (4.20) with the ansatz (4.24). With the help of the Steklov–Poincaré operator we write

$$(\gamma_1^K u_h, \gamma_0^K v_h)_{L_2(\partial K)} = (\mathbf{S}_K \gamma_0^K u_h, \gamma_0^K v_h)_{L_2(\partial K)} \,.$$

Next, we may either use the non-symmetric, see (4.7), or the symmetric, see (4.8), representation of the Steklov–Poincaré operator. According to (4.26), the non-symmetric representation leads to

$$(\gamma_1^K u_h, \gamma_0^K v_h)_{L_2(\partial K)} \approx (t_h^{(u)}, g_h^{(v)})_{L_2(\partial K)} = (\underline{g}_h^{(v)})^\top \mathbf{M}_{K,h}^\top \underline{t}_h^{(u)} = (\underline{g}_h^{(v)})^\top \mathbf{S}_{K,h}^{\mathrm{unsym}} \underline{g}_h^{(u)}$$

with

$$\mathbf{S}_{K,h}^{\mathrm{unsym}} = \mathbf{M}_{K,h}^\top \mathbf{V}_{K,h}^{-1} \left(\tfrac{1}{2} \mathbf{M}_{K,h} + \mathbf{K}_{K,h} \right) \,.$$

On the other hand, the symmetric representation with (4.27) leads to

$$(\gamma_1^K u_h, \gamma_0^K v_h)_{L_2(\partial K)} \approx (\widetilde{\mathbf{S}}_K g_h^{(u)}, g_h^{(v)})_{L_2(\partial K)} = (\underline{g}_h^{(v)})^\top \mathbf{S}_{K,h} \underline{g}_h^{(u)} \,.$$

Both matrices $\mathbf{S}_{K,h}^{\text{unsym}}$ and $\mathbf{S}_{K,h}$ originate from the same symmetric bilinear form. Whereas $\mathbf{S}_{K,h}^{\text{unsym}}$ is a non-symmetric matrix, $\mathbf{S}_{K,h}$ retains the symmetry because of its Definition (4.28).

Without saying, we have already linked the approximation order in the BEM with the one of the global FEM formulation naturally. For V_h^k in the BEM-based FEM, we have chosen $\mathscr{P}_{\text{pw}}^k(\mathscr{B}_h)$ and $\mathscr{P}_{\text{pw,d}}^{k-1}(\mathscr{B}_h)$ with the same degree k in the local BEM solver. This choice is appropriate, since the trace of functions in V_h^k on the boundary of an element lies in the used boundary element space. Furthermore, we point out that $\mathscr{P}^k(K) \subset V_h^k\big|_K$ and for a polynomial $p \in \mathscr{P}^k(K)$ it is $\gamma_0^K p \in \mathscr{P}_{\text{pw}}^k(\partial K)$ and, in particular, $\gamma_1^K p \in \mathscr{P}_{\text{pw,d}}^{k-1}(\partial K)$. Thus, the local BEM solver is exact, up to quadrature errors, for all polynomials contained in V_h^k. The choice of the boundary mesh $\mathscr{B}_h$, however, is still open. It turns out that $\mathscr{B}_h = \mathscr{T}_h(\partial K)$ is an adequate choice, i.e., the naturally given boundary mesh consisting of edges ($d = 2$) and triangular faces ($d = 3$) of the polytopal elements. This mesh is also the coarsest possible one to discretize ∂K.

The boundary element matrices only depend on the geometry and on the discretization of ∂K, but they are independent of the basis functions of the BEM-based FEM. Thus, the matrices are precomputed once per element and they are used throughout the simulation for the setup of the global FEM matrix as well as for the evaluation of all functions of V_h^k insight elements and for the approximation of their Neumann traces on the skeleton of the domain. If the mesh $\mathscr{K}_h$ consists of a few element types only, it is possible to compute the BEM matrices solely for the representative elements since they are invariant under translation and rotation. Consequently, a kind of lookup table can be used to reduce the computational cost by using the same matrices for several elements, see Sect. 6.2.6. Beside this improvement, we point out that the boundary element matrices in our application are rather small because of the coarse meshes $\mathscr{B}_h = \mathscr{T}_h(\partial K)$ and the fact that the number of nodes and the number of edges/faces is uniformly bounded, cf. Sect. 2.2.

Finally, the assembling of the global FEM matrix is performed as usual by adding up the local element-wise contributions. Here, the matrix

$$\mathbf{S}_{K,h}^{\text{unsym}} \qquad \text{or} \qquad \mathbf{S}_{K,h}$$

serves as a local stiffness matrix in the BEM-based FEM simulation.

Remark 4.7 The 2D implementation of the BEM-based FEM, used in all numerical examples in this book, utilizes $\mathbf{S}_{K,h}$ as local stiffness matrix. The entries of the boundary element matrices are computed by means of a fully numeric integration routine involving adaptive quadratures techniques. The 3D implementation, in contrary, is set up on a semi-analytic integration technique for the computation of the boundary element matrices and the assembling of the global FEM matrix is performed using $\mathbf{S}_{K,h}^{\text{unsym}}$ as local stiffness matrix. In both cases, the representation formulas are evaluated with analytic expressions. As already mentioned, the boundary element matrices are rather small. Therefore, no additional matrix

compression techniques like the Adaptive Cross Approximation (ACA) have been applied, cf. [20, 144, 148]. Furthermore, the inversion of the single-layer potential matrix $\mathbf{V}_{K,h}$ is done with the help of an efficient LAPACK [6] routine.

Local Nyström Solver

We restrict ourselves to two-dimensions and proceed as in Sect. 4.4. The boundary ∂K of a polygonal element is prescribed as a union of straight lines and can thus be parametrized by a piecewise smooth curve easily. The number of boundary segments M corresponds to the number of edges, and the vertices $\mathbf{z}_\ell$ are given by the nodes of the element. For the approximation of the bilinear form of the global FEM formulation, we proceed with the local volume integrals $(\nabla u_h, \nabla v_h)_{L_2(K)}$, since the Neumann trace $\gamma_1^K u_h$ is not accessible directly by the Nyström approximation. Consequently, the elements are subdivided into triangles and a quadrature rule is applied on each of them, where the evaluations of ∇u_h and ∇v_h are realized by means of (4.41).

The Nyström approximation has to be performed for each basis function. This involves the solution of a system of linear equations (4.39) each. In contrast, the local BEM solver only inverts one matrix per element. Furthermore, an effective generalization of the Nyström approximation to 3D is not obvious and the use of volume quadrature is unpleasant. But, the implementation of a Nyström code is much easier than the appropriate numerical approximation of the BEM matrices. Furthermore, due to the sigmoidal change-of-variables the Nyström approximation copes with singularities that appear at reentrant corners. The BEM, which is applied on the coarsest possible mesh, might need additional attention on this, see Sect. 4.5.2.2.

In order to bypass the unpleasant volume integration in the evaluation of the global FEM bilinear form using the local Nyström solver, it is possible to apply an advanced strategy. In [135], the authors have proposed a Nyström discretization using harmonic conjugates which directly gives access to the Neumann trace of the approximation. Consequently, this approach can be applied to approximate the boundary integrals $(\gamma_1^K u_h, \gamma_0^K v_h)_{L_2(\partial K)}$ in the reformulation of the FEM bilinear form such that volume integrals are avoided. Beside this, the Nyström approach relies on a piecewise smooth boundary curve only and therefore, it opens the developments towards polygonal elements with curved edges, see [5].

4.5.2 Numerical Examples and Comparison

In this section we substantiate our considerations on the local solvers. Numerical examples for the Nyström approximation as well as for the BEM have been presented in the previous sections. Furthermore, the whole book contains examples for the BEM-based FEM using the local BEM solver. Therefore, we restrict ourselves here to demonstrate the applicability of the local Nyström solver and

discuss a comparison of the two solvers in the case of the presence of singularities in the approximation space V_h^k.

4.5.2.1 Interpolation with Local Nyström Solver

To demonstrate the interpolation properties, we first interpolate the smooth function

$$v(\mathbf{x}) = \sin(2\pi x_1)\sin(2\pi x_2) \qquad \text{for } \mathbf{x} \in \Omega = (0,1)^2$$

on two different families of meshes which have already been used in a former example. The first family has been generated by the software package PolyMesher [167], and consists of convex polygons that are primarily pentagons and hexagons. The second family consist of rectangles and L-shaped elements, and has been chosen to illustrate that the presence of non-convex elements does not negatively impact the interpolation properties of the associated local spaces. The meshes with the convex and L-shaped elements are depicted in Figs. 2.14 and 2.16, respectively. The relative interpolation errors for

$$\mathfrak{I}_h^k : H^2(\Omega) \to V_h^k$$

in the H^1- as well as in the L_2-norm are presented with respect to the mesh size h in logarithmic scale in Fig. 4.4 for different approximation orders k. The results for the meshes generated by PolyMesher are visualized with a solid line whereas the results for the meshes with L-shaped elements are given with a dashed line. We observe optimal rates of convergence for both families of meshes as expected from the theory developed in Chap. 2.

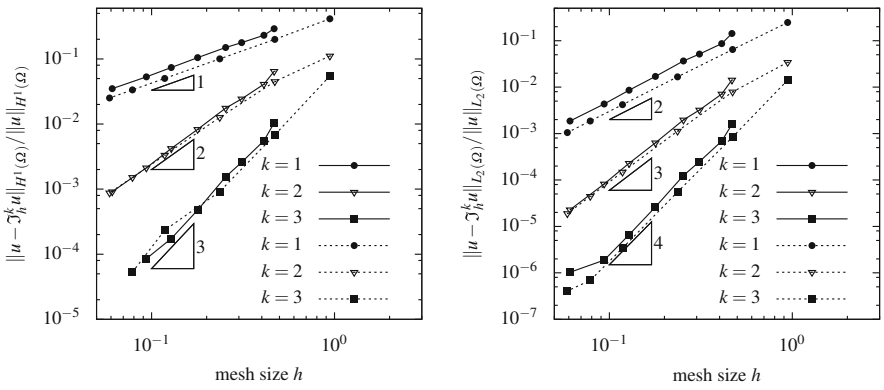

Fig. 4.4 Relative interpolation error in H^1-norm (left) and L_2-norm (right) with respect to the mesh size h on meshes produced by PolyMesher (lines, cf. Fig. 2.14) and meshes with L-shaped elements (dashed, cf. Fig. 2.16), for $k = 1, 2, 3$ and local Nyström solver

4.5.2.2 Comparison of Local Solvers for L-Domain

In a second example, we make use of polar coordinates $\mathbf{x} = (r\cos\phi, r\sin\phi)^\top$. The function

$$v(\mathbf{x}) = r^{2/3}\sin(2(\phi - \pi/2)/3) \qquad \text{for } \mathbf{x} \in \Omega = (-1,1)^2 \setminus [0,1]^2$$

is interpolated in the space V_h^1. This function exhibits the typical singularity at the reentrant corner, which is located in the origin of the coordinate system. We compare the L_2-interpolation error for three families of meshes, see Fig. 4.5, using the local Nyström solver. Afterwards, we compare the Nyström solver with a naive application of the local BEM solver and we discuss improvements.

We specify the meshes by a discretization parameter $n \sim h^{-1}$ instead of the mesh size h. The first family is denoted by $\mathscr{K}_n^1$ and the nth mesh consists of one L-shaped element, $(-1/3, 1/3)^2 \setminus [0, 1/3]^2$, and $24n^2$ squares of size $(3n)^{-1} \times (3n)^{-1}$. Thus, $\mathscr{K}_n^1$ has $(2n+1)(12n+1)+1$ vertices. The second family $\mathscr{K}_n^2$ solely consists of congruent squares of size $(3n)^{-1} \times (3n)^{-1}$ such that, the nth mesh has $27n^2$ elements. The third family $\mathscr{K}_n^3$ is obtained from $\mathscr{K}_n^2$ by agglomerating the three squares that have the origin as a vertex. The vertices in the meshes coincide with the nodes in the corresponding FEM discretization. For all square elements in either mesh, the local spaces are the bilinear functions. If K is the L-shaped element in $\mathscr{K}_n^1$, then it contains $6n+2$ nodes, i.e. degrees of freedom, on its boundary and $V_h^1|_K$ contains functions having the correct singular behaviour at the reentrant

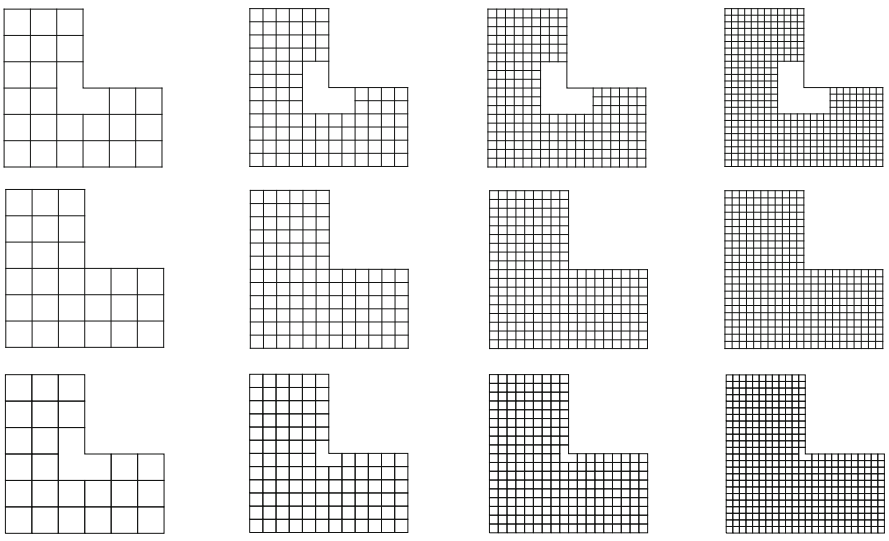

Fig. 4.5 First four meshes of first family $\mathscr{K}_n^1$ (top), second family $\mathscr{K}_n^2$ (middle), and third family $\mathscr{K}_n^3$ (bottom)

Table 4.8 Relative L_2-error (err) for interpolation in V_h^1 for the three families of meshes depicted in Fig. 4.5, and numerical order of convergence (noc) with respect to the number of degrees of freedom (DoF)

First family			Second family			Third family		
DoF	err	noc	DoF	err	noc	DoF	err	noc
40	3.24×10^{-3}	–	40	1.26×10^{-2}	–	40	3.24×10^{-3}	–
126	8.02×10^{-4}	1.22	133	4.00×10^{-3}	0.96	133	1.12×10^{-3}	0.89
260	3.55×10^{-4}	1.12	280	2.04×10^{-3}	0.90	280	5.87×10^{-4}	0.86
442	1.99×10^{-4}	1.09	408	1.46×10^{-3}	0.89	408	4.25×10^{-4}	0.86
672	1.27×10^{-4}	1.07	833	7.85×10^{-4}	0.87	833	2.32×10^{-4}	0.85
950	8.79×10^{-5}	1.06	1045	6.45×10^{-4}	0.86	1045	1.92×10^{-4}	0.84
1276	6.44×10^{-5}	1.05	1281	5.42×10^{-4}	0.86	1281	1.61×10^{-4}	0.84

corner. If K is the L-shaped element in $\mathscr{K}_n^3$, then it contains only 8 nodes, i.e. degrees of freedom, on the boundary and $V_h^1\big|_K$ also contains functions having the correct singular behaviour at the reentrant corner.

In Table 4.8, the relative interpolation error in the L_2-norm is given for all three sequences of meshes, maintaining comparable numbers of degrees of freedom between the spaces. Furthermore, the numerical order of convergence (noc) is given. This is an estimate of the exponent q in the error model $C\,\mathrm{DoF}^{-q}$. Standard bilinear interpolation theory for functions $v \in H^{1+s}(\Omega)$ on the second family of meshes yields $\|v - \mathfrak{I}_h^1 v\|_{L_2(\Omega)} = \mathscr{O}(\mathrm{DoF}^{-(1+s)/2})$, i.e. $q = (1+s)/2$. Since $v \in H^{1+s}(\Omega)$ for any $s < 2/3$, we expect to see essentially $q = 5/6$ for the second family, which is what the experiments indicate.

For the first family of meshes, we achieve $\mathscr{O}(\mathrm{DoF}^{-1})$ convergence, and we explain why this is expected. Let K denote the L-shaped element in $\mathscr{K}_{n,1}$. Since $v - \mathfrak{I}_h^1 v$ is harmonic in K, its extreme values occur on ∂K, where $\mathfrak{I}_h^1 v$ is piecewise linear and agrees with v at the vertices. We note that $v - \mathfrak{I}_h^1 v = 0$ on the two (long) edges touching the origin, so $\|v - \mathfrak{I}_h^1 v\|_{L_\infty(K)} = \|v - \mathfrak{I}_h^1 v\|_{L_\infty(\partial K_I)}$, where ∂K_I is $\partial K \setminus \partial\Omega$. Let E be an edge of ∂K_I, having length $h = 1/(3n)$. Standard 1D interpolation estimates imply that $\|v - \mathfrak{I}_h^1 v\|_{L_\infty(E)} \le h^2 \|\partial^2 v/\partial \mathbf{t}^2\|_{L_\infty(E)}$, where the derivatives are taken in the tangential direction. We deduce that

$$\|v - \mathfrak{I}_h^1 v\|_{L_2(K)}^2 \le |K| \|v - \mathfrak{I}_h^1 v\|_{L_\infty(K)}^2 \le h^4 |K| \|\partial^2 v/\partial \mathbf{t}^2\|_{L_\infty(\partial K_I)}^2 \le \tfrac{1}{3} h^4 |v|_{W_\infty^2(\Omega\setminus K)}^2 .$$

For each square element K', essentially the same argument yields

$$\|v - \mathfrak{I}_h^1 v\|_{L_2(K')}^2 \le h^6 |v|_{W_\infty^2(\Omega\setminus K)}^2 .$$

From this, we determine that

$$\|v-\mathfrak{I}_h^1 v\|^2_{L_2(\Omega)} \le \left(\tfrac{1}{3}h^4 + h^6(|\mathscr{K}_n^1|-1)\right)|v|^2_{W^2_\infty(\Omega\setminus K)} = \left(\tfrac{1}{3}h^4+\tfrac{8}{3}h^4\right)|v|^2_{W^2_\infty(\Omega\setminus K)}\,.$$

In other words, $\|v-\mathfrak{I}_h^1 v\|_{L_2(\Omega)} = \mathscr{O}(h^2) = \mathscr{O}(\mathrm{DoF}^{-1})$.

Now suppose that K is the L-shaped element in $\mathscr{K}_n^3$ with edge length h. Since the maximal interpolation error happens on the boundary ∂K, we estimate it directly by computing the linear interpolant on each edge, and comparing it with v on that edge. We determine that

$$\|v-\mathfrak{I}_h^1 v\|^2_{L_2(K)} \le 3h^2\|v-\mathfrak{I}_h^1 v\|^2_{L_\infty(K)} \le 3h^2(0.023201h^{2/3})^2 \le 0.0016149h^{10/3}\,.$$

For comparison, we estimate the interpolation error for the three $h\times h$ squares in $\mathscr{K}_n^2$ that touch the origin, namely for $K_1=[-h,0]\times[0,h]$, $K_2=[0,h]\times[-h,0]$ and for $K_3=[-h,0]\times[-h,0]$, noting that $K=K_1\cup K_2\cup K_3$. Since v is most naturally expressed in polar coordinates, we convert the bilinear interpolant $\mathfrak{I}_h^1 v$ to polar coordinates on each square, and compute upper and lower bounds on $\|v-\mathfrak{I}_h^1 v\|_{L_2(K_j)}$,

$$\|v-\mathfrak{I}_h^1 v\|_{L_2(D_j)} \le \|v-\mathfrak{I}_h^1 v\|_{L_2(K_j)} \le \|v-\mathfrak{I}_h^1 v\|_{L_2(\widehat{D}_j)}\,,$$

where D_j, $\widehat{D}_j$ are sectors of disks centered at the origin, having radii h and $\sqrt{2}h$ respectively, and satisfying $D_j\subset K_j\subset\widehat{D}_j$. These bounds are

$$0.172h^{5/3} \le \|v-\mathfrak{I}_h^1 v\|_{L_2(K_1)} = \|v-\mathfrak{I}_h^1 v\|_{L_2(K_2)} \le 0.364h^{5/3}\,,$$
$$0.571h^{5/3} \le \|v-\mathfrak{I}_h^1 v\|_{L_2(K_3)} \le 0.941h^{5/3}\,.$$

This explains why the interpolation error for the third family, while being of the same order as that of the second family, is slightly smaller.

Finally, for the first family of meshes, only the local interpolant on the (fixed) L-shaped element K, has to be approximated numerically. For the results above in Table 4.8, we used the Nyström approach. For comparison, we repeat the interpolation error experiment for the first family, using instead three versions of the local BEM solver to treat $\mathfrak{I}_h^1 v$ on K. For the first version (large edges), the boundary element mesh is precisely that suggested by K itself, consisting of two edges of length $1/3$ touching the origin, and $6n$ edges of length $h=1/(3n)$, cf. Fig. 4.6 (left). For the second version, the two long edges are each partitioned into n sub-edges of length h, cf. Fig. 4.6 (middle). As seen in Table 4.9, the convergence for the first version stagnates almost immediately, whereas the convergence for the second version is similar to what has been seen for the second and third families above. So, we see that the BEM discretization error dominates the interpolation error in these cases, but the Nyström discretization error does not. Recalling that the BEM integral formulation is attempting to compute $\gamma_1^K v$ on ∂K, and $\gamma_1^K v(\mathbf{x}) = -\frac{2}{3}r^{-1/3}$ on both

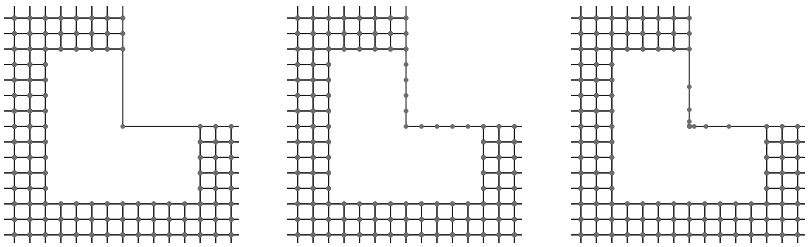

Fig. 4.6 Zoom of L-shaped element for different BEM discretizations with two large edges (left), small edges (middle) and a graded mesh (right)

Table 4.9 Relative L_2-error (err) for interpolation in V_h^1 for the first family of meshes depicted in Fig. 4.5, and numerical order of convergence (noc) with respect to the number of degrees of freedom (DoF) with three versions of the local BEM solver

Version 1 (large edges)			Version 2 (small edges)			Version 3 (graded mesh)		
DoF	err	noc	DoF	err	noc	DoF	err	noc
40	6.65×10^{-3}	–	40	6.65×10^{-3}	–	40	6.65×10^{-3}	–
126	4.88×10^{-3}	0.27	128	2.16×10^{-3}	0.97	128	1.29×10^{-3}	1.41
260	4.56×10^{-3}	0.09	264	1.10×10^{-3}	0.93	264	5.26×10^{-4}	1.23
442	4.45×10^{-3}	0.05	448	7.09×10^{-4}	0.83	448	2.64×10^{-4}	1.31
672	4.39×10^{-3}	0.03	680	5.06×10^{-4}	0.81	680	1.60×10^{-4}	1.20
950	4.36×10^{-3}	0.02	960	3.83×10^{-4}	0.81	960	1.08×10^{-4}	1.15
1276	4.34×10^{-3}	0.02	1288	3.02×10^{-4}	0.82	1288	7.75×10^{-5}	1.12

of the edges touching the origin, it is not surprising that the BEM struggles in its discretization. This challenge is mitigated for the local BEM solver by employing the a priori knowledge of the singular behaviour or by a self-adaptive procedure. We prescribe an appropriate graded mesh along the two large edges, cf. Fig. 4.6 (right), which copes with the singularity in the Neumann trace. The underlying regularity theory and the construction of graded meshes for the boundary element method has been studied in [88, 161, 171]. We repeat the convergence test with the adapted BEM discretization on the first family and retrieve the optimal rates of convergence for the interpolation error in Table 4.9.